

# UC San Diego

## UC San Diego Previously Published Works

### Title

Applying a Chemogeographic Strategy for Natural Product Discovery from the Marine Cyanobacterium *Moorena bouillonii*.

### Permalink

<https://escholarship.org/uc/item/32r1z3vp>

### Journal

Marine Drugs, 18(10)

### Authors

Leber, Christopher

Naman, C

Keller, Lena

et al.

### Publication Date

2020-10-14

### DOI

10.3390/md18100515






### Copyright Information

This work is made available under the terms of a Creative Commons Attribution License, available at <https://creativecommons.org/licenses/by/4.0/>

Peer reviewed

Article

# Applying a Chemogeographic Strategy for Natural Product Discovery from the Marine Cyanobacterium *Moorena bouillonii*

Christopher A. Leber<sup>1</sup>, C. Benjamin Naman<sup>1,2</sup> , Lena Keller<sup>1,3</sup> , Jehad Almaliti<sup>1,4</sup>, Eduardo J. E. Caro-Diaz<sup>1,5</sup>, Evgenia Glukhov<sup>1</sup>, Valsamma Joseph<sup>1,6</sup>, T. P. Sajeevan<sup>1,6</sup> , Andres Joshua Reyes<sup>7</sup>, Jason S. Biggs<sup>7</sup>, Te Li<sup>2</sup>, Ye Yuan<sup>2</sup>, Shan He<sup>2</sup> , Xiaojun Yan<sup>2</sup>  and William H. Gerwick<sup>1,8,\*</sup>

- <sup>1</sup> Center for Marine Biotechnology and Biomedicine, Scripps Institution of Oceanography, University of California San Diego, La Jolla, CA 92093, USA; cleber@ucsd.edu (C.A.L.); bnaman@nbu.edu.cn (C.B.N.); le.keller85@gmail.com (L.K.); jalmaliti@ucsd.edu (J.A.); eduardo.caro1@upr.edu (E.J.E.C.-D.); eglukhov@ucsd.edu (E.G.); valsamma@cusat.ac.in (V.J.); sajeev@cusat.ac.in (T.P.S.)
- <sup>2</sup> Li Dak Sum Yip Yio Chin Kenneth Li Marine Biopharmaceutical Research Center, Department of Marine Pharmacy, College of Food and Pharmaceutical Sciences, Ningbo University, Ningbo 315800, China; telinbu@163.com (T.L.); 23yuanye@163.com (Y.Y.); heshan@nbu.edu.cn (S.H.); yanxiaojun@nbu.edu.cn (X.Y.)
- <sup>3</sup> Department Microbial Natural Products, Helmholtz-Institute for Pharmaceutical Research Saarland (HIPS), Helmholtz Centre for Infection Research (HZI), Campus E8.1, 66123 Saarbrücken, Germany
- <sup>4</sup> School of Pharmacy, The University of Jordan, Amman 11942, Jordan
- <sup>5</sup> Department of Pharmaceutical Sciences, School of Pharmacy, University of Puerto Rico—Medical Sciences Campus, San Juan, PR 00921, USA
- <sup>6</sup> National Centre for Aquatic Animal Health, Cochin University of Science and Technology, Kochi, Kerala 682016, India
- <sup>7</sup> University of Guam Marine Laboratory, Mangilao, Guam 96923, USA; reyes.andresjoshua@gmail.com (A.J.R.); biggs.js@gmail.com (J.S.B.)
- <sup>8</sup> Skaggs School of Pharmacy and Pharmaceutical Sciences, University of California San Diego, La Jolla, CA 92093, USA
- \* Correspondence: wgerwick@health.ucsd.edu

Received: 1 September 2020; Accepted: 8 October 2020; Published: 14 October 2020



**Abstract:** The tropical marine cyanobacterium *Moorena bouillonii* occupies a large geographic range across the Indian and Western Tropical Pacific Oceans and is a prolific producer of structurally unique and biologically active natural products. An ensemble of computational approaches, including the creation of the ORCA (Objective Relational Comparative Analysis) pipeline for flexible MS<sup>1</sup> feature detection and multivariate analyses, were used to analyze various *M. bouillonii* samples. The observed chemogeographic patterns suggested the production of regionally specific natural products by *M. bouillonii*. Analyzing the drivers of these chemogeographic patterns allowed for the identification, targeted isolation, and structure elucidation of a regionally specific natural product, doscadenamide A (**1**). Analyses of MS<sup>2</sup> fragmentation patterns further revealed this natural product to be part of an extensive family of herein annotated, proposed natural structural analogs (doscadenamides B–J, 2–10); the ensemble of structures reflect a combinatorial biosynthesis using nonribosomal peptide synthetase (NRPS) and polyketide synthase (PKS) components. Compound **1** displayed synergistic in vitro cancer cell cytotoxicity when administered with lipopolysaccharide (LPS). These discoveries illustrate the utility in leveraging chemogeographic patterns for prioritizing natural product discovery efforts.

**Keywords:** *Moorena bouillonii*; marine natural products; chemogeography; metabolomics

## 1. Introduction

Natural products discovery programs operate with the general goal of detecting and characterizing chemically unique or biologically active substances. A common obstacle in discovery efforts is the rediscovery of known compounds, suggesting a need for tools and techniques that allow researchers to give priority to samples that possess new or otherwise interesting chemical substances. Various strategies have been employed for the dereplication of known chemicals within samples, and for the prioritization of samples based on chemical composition. In this regard, mass spectrometric analyses, usually in combination with liquid chromatography (e.g., LC-MS), have found great utility in natural products research due to the rapidity, small sample size requirements, and high amount of data generated. As a result, a number of approaches and algorithms have been developed to sift through LC-MS data so as to rapidly detect molecules of greater structural novelty and interest.

PoPCAR (Planes of Principal Component Analysis in R) applies principal component analysis (PCA) to a processed bucket table of sample features, selects outlying samples across different PCA planes, and then leverages the PCA feature loadings to identify the features that make the outlying samples unique [1]. IDBac integrates proteomics and metabolomics data captured via MALDI-TOF MS applied to bacterial colonies on agar plates to classify bacterial strains and distinguish between closely related strains [2]. Global Natural Products Social Molecular Networking (GNPS) is a platform that facilitates the sharing of mass spectral data and provides tools for performing MS<sup>2</sup>-based networking analyses [3]. GNPS continues to expand the repertoire of innovative approaches and techniques that it offers, with recent additions including a pipeline for Feature-Based Molecular Networking (FBMN) [4]. FBMN utilizes a processed bucket table of sample MS<sup>1</sup> features in conjunction with MS<sup>2</sup> fragmentation data to produce highly sensitive molecular networks well suited for quantitation and differentiation of isomeric compounds. In addition to these more specific tools, multiple tools are available for the processing and/or statistical analyses of MS-based chemical profile data, including XCMS [5], MZmine [6], and Metaboanalyst [7]. The GNPS classical molecular networking approach [3] is of particular note. While many approaches are sensitive to sample set heterogeneity and rely on specific or consistent sample preparations and data acquisitions in order to provide appropriate results, the classical molecular networking approach is much more flexible, and its outcomes are insulated from imperfect data. This allows classical molecular networking to be used in analyzing datasets that vary across numerous dimensions (instrument type, chromatographic method, sample preparation, etc.), providing many more opportunities for connecting disparate data sources.

The cyanobacterial genus *Moorena* (previously *Lyngbya*, then *Moorea*) is a prolific source of biologically active natural products, with biosynthetic gene clusters accounting for 18% of *Moorena* spp. genomes, on average [8–10]. Consistent with this finding, some 70 different isolated and structurally defined compounds have been reported from *M. bouillonii* (Table S1) [11–44]. These display a broad structural diversity, and include peptides [41], cyclodepsipeptides [16], macrolides [12] and glycosidic macrolides [35], and lipids [43]. These compounds are also notable for their biological activities, including cytotoxins such as bouillonamide [23], lyngbouilloside [35], multiple lyngbyabellins [12,13], and the exquisitely potent apratoxin A [16]. Other *M. bouillonii* compounds have been reported with cannabimimetic properties, such as columbamides A–C [25] and mooreamide A [43], or as modulators of intracellular calcium mobilization such as alotamide A [14]. *M. bouillonii* has a wide distribution across the tropical Western Pacific and Indian Oceans. However, *M. bouillonii* metabolites have only been described from collections made from a limited number of discrete locations, including Papua New Guinea [14,19,23,25,28,33–35,39,41,43], Guam [11,12,15,16,18,20,22,24,29,36,37,42], Palau [11,18,38,40,44], Malaysia [26,27], Palmyra Atoll [13,21], Fiji [31] (The organism in this manuscript is reported as *M. producens*, however the manuscript includes a photo of the organism, which displays a morphology characteristic of shrimp-woven *M. bouillonii*. The 16S rRNA gene-based classification was inconclusive and known compounds previously isolated from *M. bouillonii* were reported.), the Red Sea [17] (The organism in this manuscript is reported as *M. producens*, however the 16S rRNA gene-based classification is inconclusive and known chemistry associated with *M. bouillonii* was

reported.), and the islands of southern Japan [30,32]. Collections from these diverse geographical regions differ substantially in their composition of metabolites, suggesting that even though many compounds are already known from *M. bouillonii*, comparing samples of different geographical origin could reveal distributional patterns in chemodiversity that would facilitate the identification of new natural products.

Much of the previous work connecting natural products chemistry and geography has focused on the latitudinal herbivory-defense hypothesis (LHDH). The LHDH suggests that tropical species display more developed defense phenotypes (including chemical defenses) than temperate species, due to higher levels of biotic stressors [45–47]. Studies in both terrestrial organisms [45–48] and marine organisms [49–51] lend support to this hypothesis, but many examples counter to LHDH have also been reported, layering the theory with some degree of controversy while also revealing the complexity of drivers that influence chemical defense [52,53]. Orthogonally, it has become a common strategy to look in underexplored geographical locations in order to find new and unique natural products. This has led natural products discovery efforts to interesting and exotic habitats, including tropical coral reefs [11–44], hypersaline lakes [54], the Arctic [55] and Antarctic [56], hydrothermal vents [57], and the deep sea [58]. In spite of the acknowledgement that sampling in new geographical locations can allow access to new natural products, there are few examples of systematically applying geographical knowledge in order to inform natural product discovery. However, in one study the crude extracts and fractions from 300 geographically and taxonomically diverse cyanobacterial and algal collections were profiled by LC-MS/MS [59]. Analyses by GNPS classical molecular networking revealed geographic hotspots for chemodiversity, thus allowing for a molecular feature to be prioritized based on its chemogeographical distribution. In this case, it led to the characterization of a new metabolite given the common name yuvalamide A. Another example study focused on cyanobacteria from one specific genus, analyzing 10 samples of *Symploca* spp. collected at different times and in different places. This led to the efficient and targeted discovery of a new sample-specific bioactive natural product, samoamide A [60].

In the present study, we illustrate the value of leveraging geographical patterns in chemodiversity to find previously uncharacterized natural products and apply this strategy to the marine filamentous cyanobacterial species *M. bouillonii*. This is a particularly interesting organism because of its wide geographical range and richness in natural products. To enable analyses and inform current discovery efforts based on legacy data, we were inspired to develop a flexible data pipeline described as the Objective Relational Comparative Analysis (ORCA) of chemical profiles from LC-MS data. Analyses of the LC-MS profiles from geographically disparate chemical extracts of *M. bouillonii*, used in conjunction with GNPS classical molecular networking, allowed for the prioritization of a molecular feature that led to the isolation and characterization of a new compound we called laulauamide (**1**). (The discovery, isolation, and structure elucidation of **1** were presented at the 2017 Annual Meeting of the American Society of Pharmacognosy. The name laulauamide was used for a poster presentation, and the associated abstract can be found under abstract P-219 at the following link [[http://asp2017.org/wp-content/uploads/2016/12/ASP20201720Annual20Meeting\\_web.pdf](http://asp2017.org/wp-content/uploads/2016/12/ASP20201720Annual20Meeting_web.pdf)]). Molecular networks along with detailed MS<sup>2</sup> fragmentation analyses revealed the presence of an extensive collection of proposed natural analogs. These display diversification through varied combinations of fatty acid side chains at two locations. Assays for biological activity yielded synergistic cytotoxic activity between **1** and lipopolysaccharide (LPS). Late in the performance of this work, a manuscript appeared from another laboratory that reported the isolation and structure elucidation of the main component of this new natural product family, and assigned it the common name “doscadenamide A” [29], a name we retain so as to not create confusion in the literature record.

## 2. Results and Discussion

To allow for the comparison of LC-MS traces of extracts from different collections of *M. bouillonii*, a new pipeline was created called the Objective Relational Comparative Analysis (ORCA) pipeline

(<https://github.com/c-leber/ORCA>) (Figure 1). ORCA is a flexible, modular pipeline that includes capabilities for simple and customizable MS<sup>1</sup> feature processing. ORCA can also accept any bucket table of samples vs. features as input, allowing for the comparison of data from any source that can be tabulated in such a manner. To accommodate heterogeneous data and to allow for the comparison of diverse datasets, ORCA MS<sup>1</sup> feature processing starts with an input directory of mzXML files, from which the MS<sup>1</sup> features are picked and integrated based on the mass-to-charge ratio ( $m/z$ ) and a user-selected variant of retention time (rt). Feature picking is parameterized with the user-defined  $m/z$  and rt tolerances, and the peak size and shape parameters. Subsequently, MS<sup>1</sup> features picked from each sample file are consolidated based on the user-defined  $m/z$  and rt tolerance parameters and are organized into a samples vs. features bucket table containing feature integration values, with options to apply transformations based on the goals of the downstream analyses.

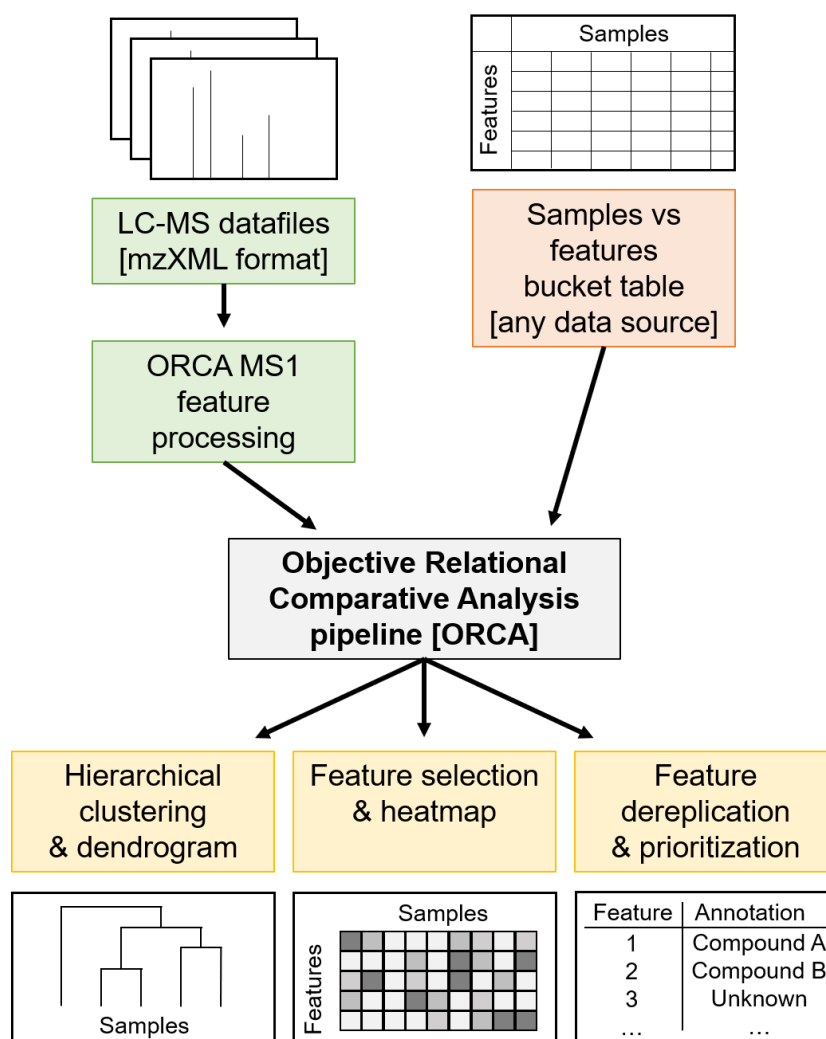


**Figure 1.** Illustration of the Objective Relational Comparative Analysis (ORCA) pipeline. The pipeline accepts inputs of either LC-MS datafiles in mzXML format, which can then undergo MS<sup>1</sup> feature processing, or an externally created samples vs. features bucket table coming from any data source. Analyses currently offered as a part of the ORCA pipeline include hierarchical clustering, feature selection, and feature dereplication based on user-provided reference data.

After processing of the sample MS<sup>1</sup> features, or the input of an externally generated sample vs. feature bucket table, the vectors of the feature values can then be utilized to initiate a diverse array of analyses, including hierarchical clustering of the samples to gain insights into the relationships between the samples, and univariate feature selection to learn about what specific MS<sup>1</sup> features

are driving the differences between groups of samples. These analyses can then be visualized as dendrograms or heat maps, respectively. ORCA can also be used to generate a list of the most prominent MS<sup>1</sup> features across samples and to assign putative identifications from a user-supplied spreadsheet, allowing one to efficiently detect expected peaks across many samples, and to quickly determine the mass spectral signature of new potential isolation targets. ORCA was designed for assessing the relationships between heterogeneous samples and generating hypotheses regarding which features are driving these relationships; this makes ORCA a useful framework for not only learning about chemogeographical patterns, but also for comparing chemical profiles across different growth conditions [61], detecting contamination of botanical extracts [62], identifying chemotaxonomic patterns [63], and many other potential uses.

Crude extracts of field-collected samples of *M. bouillonii* from American Samoa, Guam, Kavaratti (Lakshadweep Islands, India), Saipan, and the Paracel Islands (Xisha) in the South China Sea, as well as an in-house culture from Papua New Guinea, were profiled via LC-MS/MS; the resultant chromatograms were used as inputs for MS<sup>1</sup> feature processing in ORCA. Hierarchical clustering was performed on the MS<sup>1</sup> features and a dendrogram was produced with a cophenetic correlation coefficient of 0.905, indicating that the displayed structure in the dendrogram is highly correlated to the cosine distances between samples, and thus is representative of the data (Figure 2). The structure in the dendrogram suggests clustering of samples according to geographical region, a phenomenon that has previously been observed across other cyanobacterial samples [59] but has not been specifically reported as a pattern for *M. bouillonii*. It is worth noting that, while samples with shared geographical origin are indeed arranged in clusters together in the dendrogram, the branch points for each geographical cluster are quite large, ranging from 0.4763 cosine distance for the two samples from Guam to 0.7248 cosine distance for where the three samples from Saipan converge. This is likely the result of a combination of the high variability and complexity in the composition of the studied samples, as well as the “curse of dimensionality” that artificially enlarges distance values when large numbers of features are being considered [64]. Classical molecular networking analysis using GNPS provided an orthogonal view, supporting the idea of chemogeographical specificity in these *M. bouillonii* samples, as numerous clusters of location-specific nodes are visible in the resultant network (Figure 3 and Figure S1). Furthermore, hierarchical clustering performed on presence-absence data of the MS<sup>2</sup> nodes from GNPS, as visualized with a dendrogram (Figure 4), revealed a chemogeographical clustering similar to that produced from the ORCA MS<sup>1</sup> features (Figure 2). The geographically associated structure in the data, as observable via both ORCA dendrograms, along with the presence of numerous location-specific clusters in the molecular network, led us to generate the hypothesis that the geographically specific distributions of natural products in our samples could be leveraged to identify previously unreported metabolites. The clustering of samples by specific geographical location stimulated further analyses to determine which molecular features were driving the observed geographic clusters, and which peaks were regionally specific. Particular attention was paid to Saipan, as it represented one region from which no new natural products from *M. bouillonii* had been reported in the scientific literature.

One cluster in the GNPS molecular network comprising only nodes originating from the Saipan-collected samples contained a particularly intense node for a feature with  $m/z$  457.785 (Figure 3). Further investigations in ORCA revealed that this feature was present in high abundance in all samples from Saipan but was undetected or detectable at very low levels in the MS<sup>1</sup> spectra of samples from all the other studied locales (Table S2). Additionally, this feature was not dereplicated when queried against all published compounds from *M. bouillonii* at the time (Table S3) and when searched against the MarinLit database (<http://pubs.rsc.org/marinlit/>). This intriguing chemogeographic pattern prompted prioritization of this feature for isolation and structure elucidation, ultimately resulting in the characterization of a region-specific metabolite. Based on the specific collection site from which the Saipan samples originated (Laulau Bay, Saipan), we originally termed this metabolite “laulauamide”. A molecular feature with  $m/z$  721.10 was found to have a very similar geographic distribution. It was

detected with high intensity in samples from Saipan, while being undetected or detectable at very low levels in other samples (Table S2), and thus was another strong driver of the clustering of the Saipan samples. Isolation and analytical characterization revealed that this MS feature was the sodiated adduct of the known compound lymbbyapeptin A [41] (Table S3).

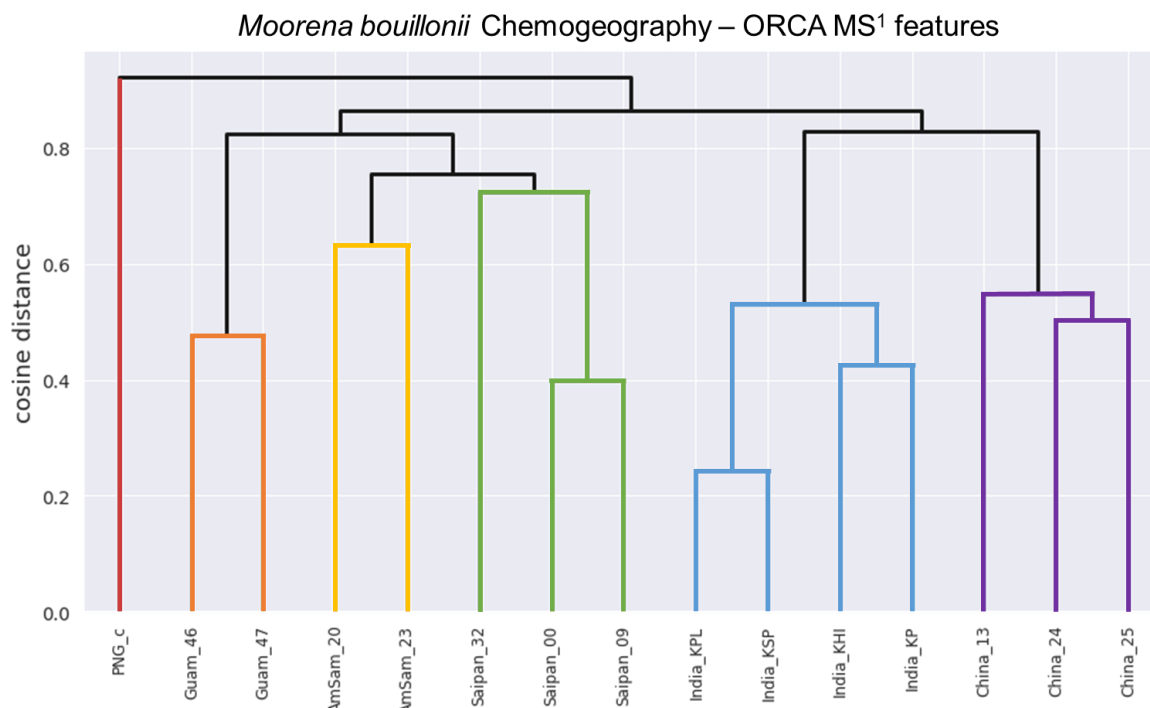


**Figure 2.** ORCA-generated dendrogram (cophenetic correlation coefficient = 0.905) displaying the results of hierarchical clustering of the MS<sup>1</sup> features from *M. bouillonii* crude extracts. Samples are labeled with aliases comprising a general collection location concatenated to an abbreviated sample code. The structure in the dendrogram suggests that samples collected from the same geographical area are chemically more similar. Colorized for emphasis. Red: Papua New Guinea; Orange: Guam; Gold: American Samoa; Green: Saipan; Blue: Kavaratti (Lakshadweep Islands, India); Purple: Paracel Islands (Xisha) in the South China Sea.

*M. bouillonii* biomass (1 L sample, 132 g dry biomass yielding 10 g of crude extract) from Saipan's Laulau Bay (denoted as Saipan\_32 in Figures 2 and 4) was thoroughly extracted with 2:1 dichloromethane and methanol, and the resulting crude extract was fractionated over silica using vacuum liquid chromatography. LC-MS/MS analysis of the fractions revealed the MS<sup>1</sup> feature of interest to be in highest abundance in two relatively polar fractions. Reverse phase HPLC was used to initially isolate 1.5 mg of this compound from the two fractions. 1D and 2D NMR experiments were utilized to establish the planar structure of **1**, with major contributions from the <sup>1</sup>H-<sup>1</sup>H Correlated Spectroscopy (COSY), <sup>1</sup>H-<sup>13</sup>C Heteronuclear Single Quantum Coherence (HSQC), <sup>1</sup>H-<sup>13</sup>C Heteronuclear Multiple Bond Coherence (HMBC), HSQC-Total Correlation Spectroscopy (TOCSY), and long-range <sup>1</sup>H-<sup>13</sup>C Heteronuclear Single Quantum Multiple Bond Coherence (HSQMBC) data.

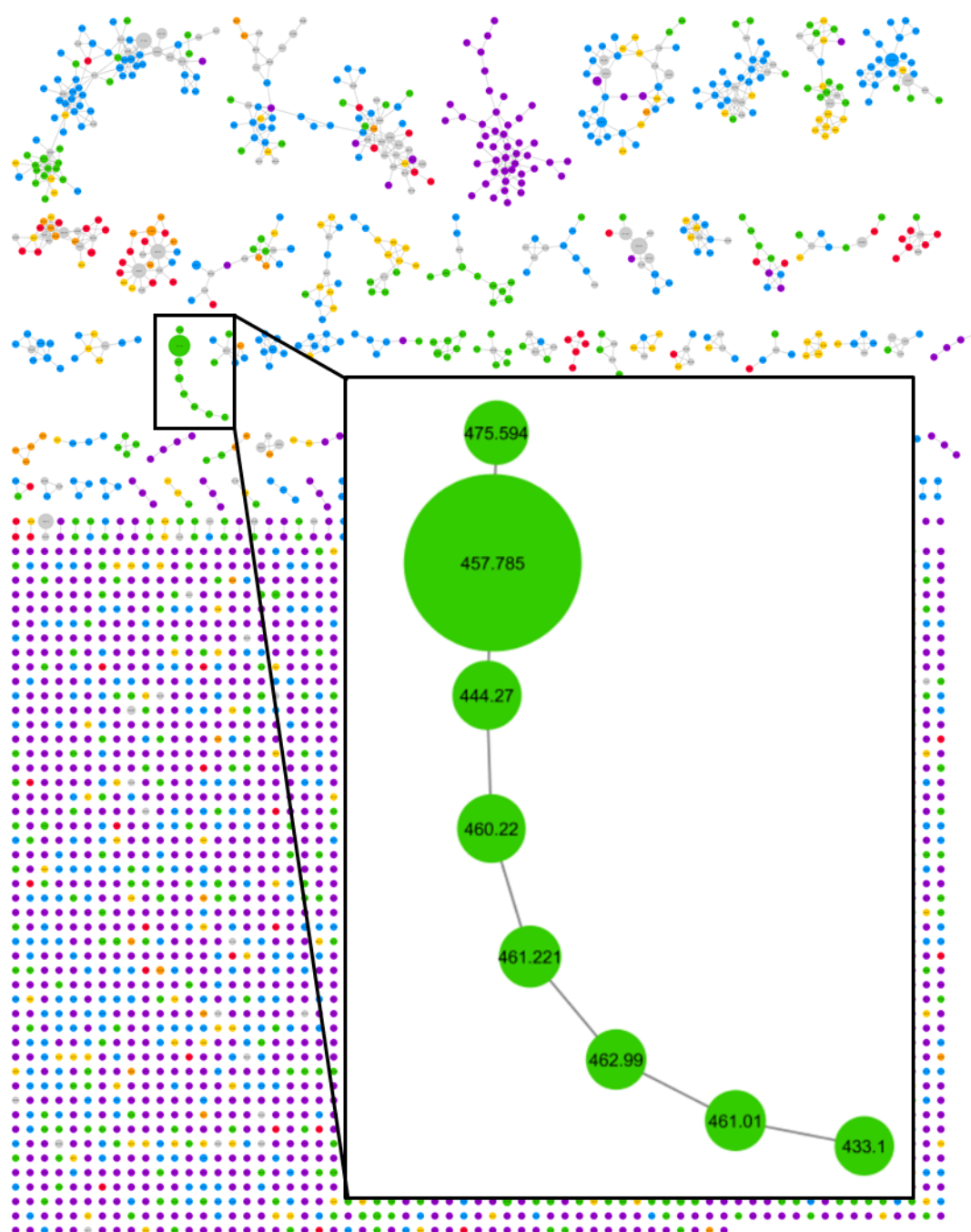


**Figure 3.** Global Natural Products Social Molecular Networking (GNPS) classical molecular network of fifteen *M. bouillonii* crude extracts with the enlarged inset showing a cluster containing **1** (denoted with precursor mass  $m/z$  457.785) and seven other nodes representing potential doscadenamide analogs (based on LR-MS/MS data). The green coloring of the nodes indicates that they represent features only detected in samples from Saipan. Nodes are scaled to summed precursor intensity. Grey nodes represent the MS<sup>2</sup> features that are present in samples from more than one geographical region. Geographical location of samples is colorized as follows: Red: Papua New Guinea; Orange: Guam; Gold: American Samoa; Green: Saipan; Blue: Kavaratti (Lakshadweep Islands, India); Purple: Paracel Islands (Xisha) in the South China Sea.



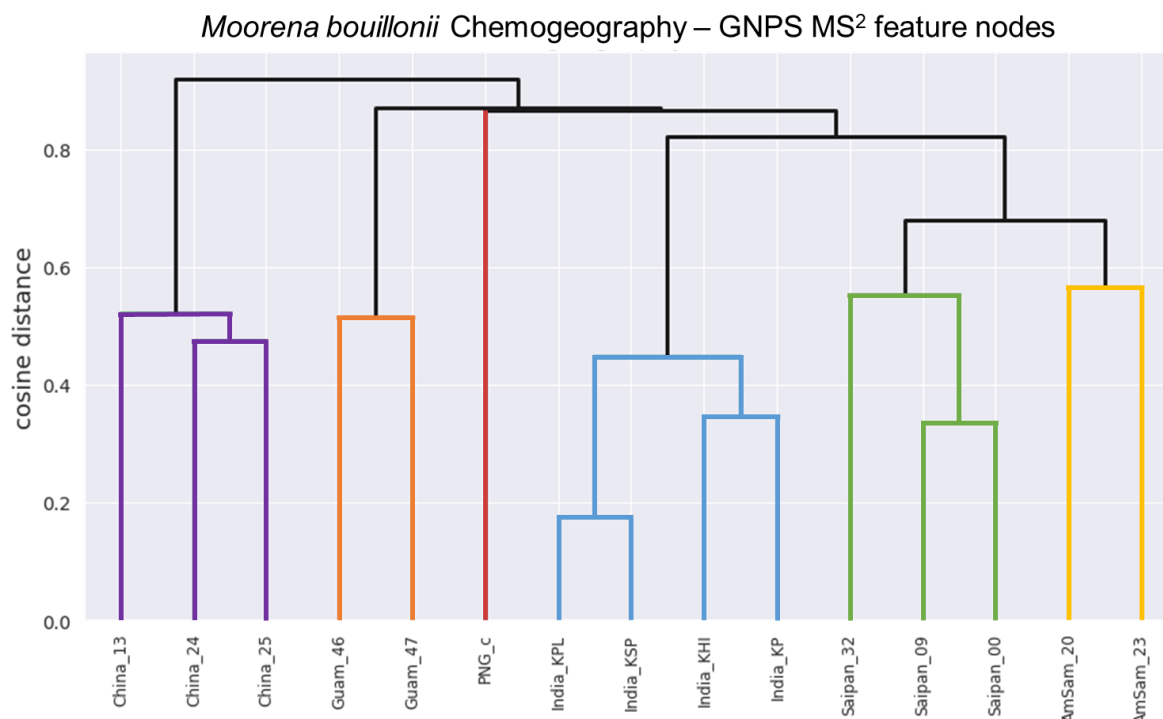


**Figure 4.** ORCA-generated dendrogram (cophenetic correlation coefficient = 0.960) displaying the results of hierarchical clustering of the *M. bouillonii* crude extracts presence–absence data regarding GNPS nodes. Samples are labeled with aliases comprising a general collection location concatenated to an abbreviated sample code. Similar to Figure 2, the structure in the dendrogram suggests that samples collected from the same geographical area are chemically more similar. Colorized for emphasis. Red: Papua New Guinea; Orange: Guam; Gold: American Samoa; Green: Saipan; Blue: Kavaratti (Lakshadweep Islands, India); Purple: Paracel Islands (Xisha) in the South China Sea.

The <sup>1</sup>H and <sup>13</sup>C NMR chemical shifts for the two acetylene groups were highly similar, and by HMBC correlations both had an adjacent methylene group at the same shift ( $\delta$  2.18, H<sub>2</sub>-15 and H<sub>2</sub>-24). In one of these two cases, sequential correlations deduced from the <sup>1</sup>H-<sup>1</sup>H COSY data, and supported by the results of a <sup>1</sup>H-<sup>13</sup>C HSQC-TOCSY experiment, provided a spin system involving three additional shielded methylene groups at  $\delta$  1.44, 1.39, and 1.75 and 1.42 (H<sub>2</sub>-23, H<sub>2</sub>-22, and H<sub>2</sub>-21). The final of these methylene groups was positioned adjacent to a deshielded methine group at  $\delta$  3.75 (H<sub>2</sub>-20). By COSY, the methine was determined to be adjacent to a shielded methyl group at  $\delta$  1.12 (H<sub>3</sub>-27), and its chemical shift was explained by an HMBC correlation placing it adjacent to an ester or amide carbonyl ( $\delta$  176.4, C-19). The spin system of the second acetylene-terminating partial structure was highly similar and partially overlapped but terminated with a more shielded methine proton at  $\delta$  2.13 (H-11) with an adjacent methyl group ( $\delta$  1.11, H<sub>3</sub>-18) and amide or ester carbonyl ( $\delta$  177.0, C-10). Summarizing, two essentially identical 2-methyl-7-octynoic acid structural units were thus defined from highly similar but non-identical data subsets.

The remainder of the molecule was thus composed of C<sub>9</sub>H<sub>14</sub>N<sub>2</sub>O<sub>2</sub> with 3 degrees of unsaturation resulting from an enone and one ring structure. Two <sup>1</sup>H NMR singlets ( $\delta$  5.04, H-2 and 3.84, H<sub>3</sub>-9) along with a 9-proton connected spin system remained unassigned. The singlet at 3.84 ppm was assignable to a methoxy group at the  $\beta$ -position of the enone by virtue of its relatively deshielded chemical shift and HMBC correlations to the highly deshielded olefinic carbon at  $\delta$  179.2 (C-3). The other singlet was thus assigned to the  $\alpha$ -position of this enone as it was attached to a shielded olefinic carbon at  $\delta$  94.2 (C-2) and showed an HMBC correlation to the carbonyl carbon at  $\delta$  170.0 (C-1). As this partial structure accounted for all oxygen atoms in compound **1**, the shielded nature of this carbonyl necessarily required

it to be attached to a nitrogen atom, forming an amide. Based on  $^1\text{H}$  and  $^{13}\text{C}$  NMR chemical shift data ( $\delta$  4.64, H-4;  $\delta$  59.2, C-4), one terminus of the remaining spin system was assigned to a methine with an attached nitrogen atom.  $^1\text{H}$ - $^1\text{H}$  COSY data, in conjunction with the  $^1\text{H}$ - $^{13}\text{C}$  HSQC-TOCSY, allowed formulation of four sequential methylene groups. The final methylene was also relatively deshielded ( $\delta$  3.22 and 3.13, H<sub>2</sub>-8;  $\delta$  39.3, C-8), consistent with its attachment to a nitrogen atom. At this point, all atoms in the molecular formula of compound **1** were accounted for, except for one proton that was attached to a heteroatom by evaluation of the HSQC data (e.g., only 39 protons were found attached to carbon atoms); this was deduced to be an NH as three of the four oxygen atoms were assigned as carbonyls and one as a methylated enol.

HMBC correlations from the two diastereotopic protons at  $\delta$  3.13/3.22 ppm (H<sub>2</sub>-8) to the carbonyl at  $\delta$  177.0 (C-10) connected these two partial structures. The other 2-methyl-7-octynoic acid was therefore connected to the only remaining heteroatom, the N-atom connected to the  $\delta$  170.0 (C-1) carbonyl of the enone functionality. Remaining structural features at this point included the formation of one ring, and placement of a proton on one of the two nitrogen atoms; two possibilities emerged (**1a** and **1b**) (Figure 5).

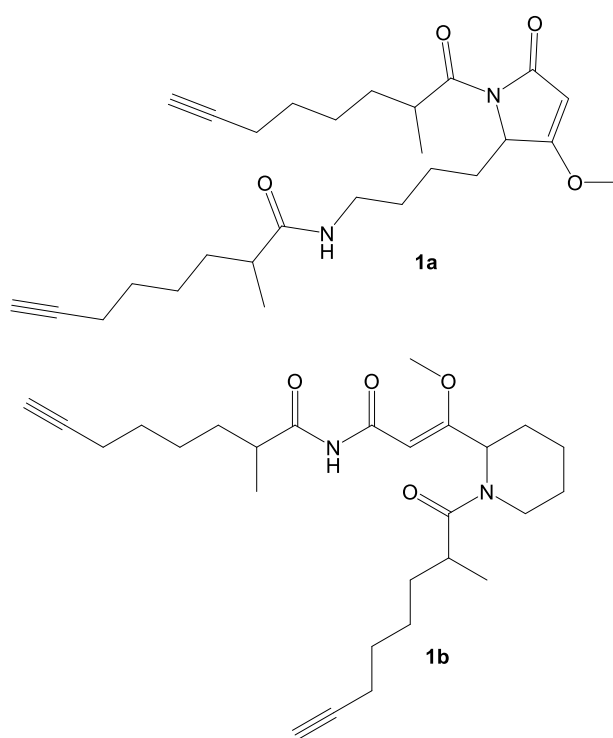


**Figure 5.** Competing structural hypotheses for the two-dimensional structure of compound **1**.

Both structural possibilities had features that were attractive and unattractive from a predicted biosynthetic perspective. In **1a**, the fundamental assembly of the PKS derived octynoic acid; its passage to an NRPS to incorporate a lysine residue, followed by a ketide extension, *O*-methylation of the  $\beta$ -enol, and cyclization to a pyrrolidone ring, is well preceded within cyanobacterial natural products [65–67]. However, the acylation of a second octynoic acid residue to the lysine side chain nitrogen is an unprecedented event. Alternative structure **1b** has the attractiveness of a regular, predicted PKS(4)-NRPS(glycine)-PKS(3)-NRPS(glycine)-PKS architecture; however, it is quite awkward in requiring several unusual adjustments to the oxidation state of the carbon atoms, and creation of the second 2-methyl-7-octynoic acid residue via a completely different set of biosynthetic steps from the first one.

Modeling of these two alternative cyclization products for  $^{13}\text{C}$  NMR shifts (see Figures S2 and S3 for the predicted  $^{13}\text{C}$  NMR shifts for **1a** and **1b**, respectively) and comparison with those experimentally

measured for **1** revealed that both possibilities were reasonably good fits, but the predicted values for **1a** tended to be closer to the shifts experimentally derived for compound **1**. For both C-2, the methyl enol carbon (**1a**  $\delta$  95.5, **1b**  $\delta$  101.4, **1**  $\delta$  94.2), and C-3, the deshielded olefinic carbon (**1a**  $\delta$  180.7, **1b**  $\delta$  171.5, **1**  $\delta$  179.2), the fit for alternative **1a** was considerably better. Only at C-6 was the cyclization product proposed in **1b** favored (**1a**  $\delta$  24.3, **1b**  $\delta$  19.6, **1**  $\delta$  20.4). A deeper look into the long-range  $^1\text{H}$ - $^{13}\text{C}$  HSQMBC data was undertaken. The key proton distinguishing these two possible structures, H-4 at  $\delta$  4.64, showed correlations to several resonances, including two of the three carbonyl resonances ( $\delta$  170.0, C-1;  $\delta$  176.4, C-19) and the  $\beta$ -oxygenated enone ( $\delta$  179.2, C-3); these correlations were compatible with structure **1a** (one 2-bond and two 3-bond correlations), while in structure **1b** these correlations would result from one 2-bond, one 4-bond, and one 6-bond  $^1\text{H}$ - $^{13}\text{C}$  coupling. Furthermore, analysis of the HMBC correlations observed for H-4 and H<sub>2</sub>-8, both from the lysine-derived residue, showed mutual signals with only C-5 at  $\delta$  29.0 and C-6 at  $\delta$  20.4 that would be consistent with either proposed structure. There were no shared correlations observed between these protons and the equally 3-bond proximal carbonyl in **1b**, nor 3-bond correlations from H-4 to C-8 and H-8 to C-4 that would be reasonably expected to be observed from **1b**, lending further support for **1a** as being the correct structure of **1**.

Compound **1** contains three stereocenters—two associated with the two 2-methyl-7-octynoic acid side chains, and one contained in the central heterocycle. A racemic standard of 2-methyloctanoic acid was derivatized with (*S*)-(+)-2-phenylglycine methyl ester. A chiral standard of (*S*)-2-methyloctanoic acid was generated via the zirconium-catalyzed asymmetric carbo-alumination (ZACA) reaction [68] of 1-octene to stereoselectively install a methyl group at the C-2 position, followed by an oxidation to 2-methyloctanoic acid and derivatization with (*S*)-(+)-2-phenylglycine methyl ester. Configuration of both 2-methyloctynoic acid moieties of compound **1** was established to be *R* through catalytic hydrogenation, acid hydrolysis, derivatization with (*S*)-(+)-2-phenylglycine methyl ester, and comparison via LC-MS to the generated standards of 2-methyloctanoic acid coupled with the same chiral auxiliary group (Figure S4). Ozonolysis with an oxidative work-up [69], followed by acid hydrolysis, was used to open the heterocyclic ring structure and liberate lysine from compound **1**. The lysine was then derivatized with Marfey's reagent (*L*-FDAA) and compared to racemic and *L*-lysine standards derivatized with the same Marfey's reagent, indicating an *S* configuration of this residue (Figure S5). The fully elucidated structure of compound **1** was thus determined as in Figure 6.

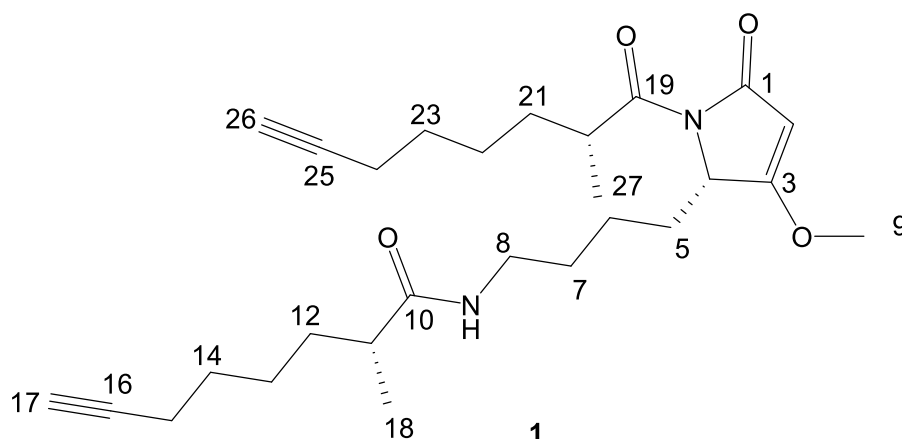
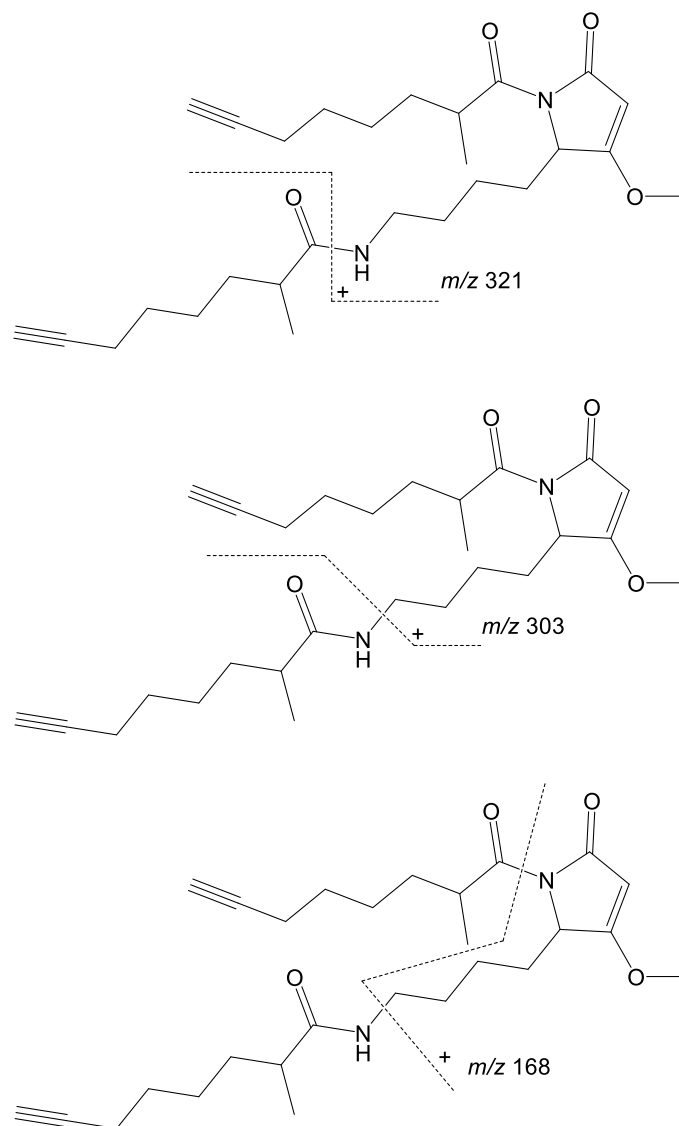


Figure 6. Complete structure of compound **1**.

Low-resolution LC-MS/MS fragmentation data for **1** consistently showed three peaks at  $m/z$  321, 303, and 168 (Figure S6), which we predicted to represent a side-chain loss, a side-chain loss plus the loss of an amine, and the loss of both side chains plus an amine, respectively. To better understand the fragmentations of compound **1** and use this information for identifying analogs based on repeating the MS<sup>2</sup> fragmentation patterns, high-resolution MS<sup>2</sup> fragmentation data were acquired for compound **1**. Numerous fragment peaks were recorded, including peaks observed at

$m/z$  321.2171, 303.1901, and 168.1016. These values match very well to the calculated monoisotopic masses of the predicted fragment structures shown in Figure 7 ( $m/z$  321.217, 303.183, 168.102; allowing for hydrogen rearrangements), lending support to our fragmentation hypothesis, and providing a starting point for understanding and proposing the structures of analogs via their fragmentation patterns.



**Figure 7.** Hypothesized fragment structures of compound 1.

GNPS classical molecular networking placed compound 1 as a node in a cluster with seven other nodes originating from the Saipan *M. bouillonii* samples (Figure 3), suggesting several naturally occurring analogs were present. ORCA revealed that compound 1 is also present in samples from Guam, though detected with a much lower MS<sup>1</sup> intensity than in samples from Saipan. This inspired the generation of a more detailed molecular network composed of both crude extracts and fractions from a Saipan sample and a Guam sample (denoted as Saipan\_32 and Guam\_46 in the above dendrograms), revealing an even larger cluster of potential analogs that contained 33 nodes, including compound 1 (Figure S7). Some nodes in the cluster had very similar masses, which could be the result of an artifact from the particular parameter set selected for the analysis, an artifact of the low resolution MS data analyzed, or be an indicator of isomeric analogs; therefore, further analysis was needed.

Analysis using the GNPS in browser network visualizer suggested that there was a common connection between many of the potential analogs (23 out of 33, including 1), namely the presence of an

MS<sup>2</sup> fragment peak at  $m/z$  168 (Figure S7). To facilitate further analysis of MS<sup>2</sup> spectra and the presence of potential analogs, the ORCA MS<sup>2</sup> auxiliary pipeline was developed. MS<sup>2</sup> scans from the Saipan and Guam crude extract and fractions were binned based on precursor mass, and then filtered to only precursor masses with scans that included a  $m/z$  168 fragment peak. Clustering scans from each relevant precursor mass by cosine distance, paired with manual analysis, allowed the structures of 9 analogs (2–10) to be proposed (Figure 8; see Figures S8–S26 for the proposed structures, consensus spectra, and predicted fragment structures). It must be noted that alternative structural proposals are conceivable for these analogs; however, given the literature precedent for cyanobacteria to produce families of natural products with the same array of variations in desaturation and oxidation as proposed here, e.g., [66,70,71], and the predictable MS<sup>2</sup> fragmentation spectra observed, these proposals represent the most parsimonious and best supported structural hypotheses. Ambiguities in the remaining related MS<sup>2</sup> spectra prevent the definitive assignment of carbon chain isomers and positional isomers, and the proposal of additional analogs, but suggest a process of combinatorial biosynthesis in generating this expansive natural product family. While quantities of these minor metabolites in our samples were not sufficient for isolation and further characterization, the total synthesis published alongside the characterization of **1** [29] is very amenable to incorporating alternative side chains, and this could be used for generating these proposed analogs for further study.

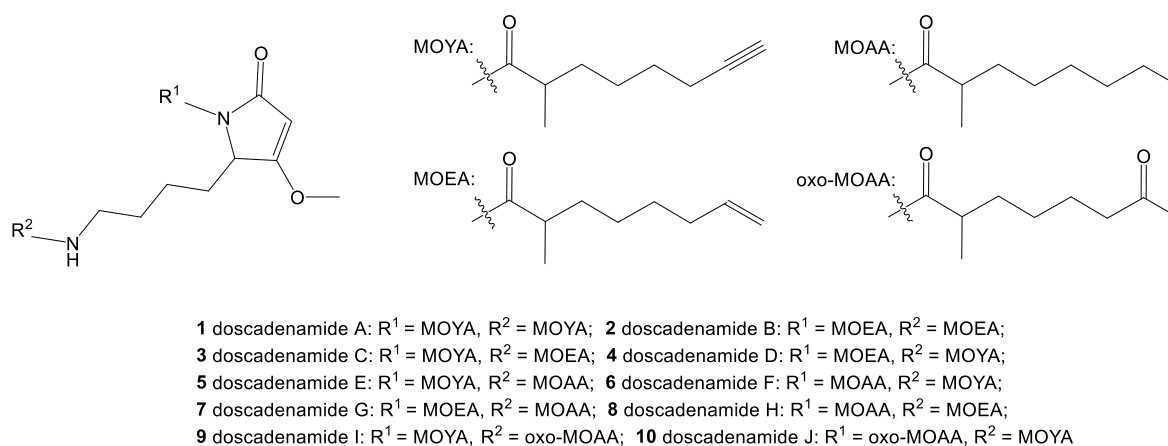


**Figure 8.** The doscadenamides: compound **1**, along with its analogs whose proposed structures were annotated via informative patterns in the MS<sup>2</sup> fragmentation data (see Figures S9–S26). Each analog consists of a heterocyclic core with two fatty acid side chains with the following possibilities: MOYA = 2-methyl octynoic acid; MOEA = 2-methyl octenoic acid; MOAA = 2-methyl octanoic acid; oxo-MOAA = 2-methyl 7-oxo octanoic acid.

Compound **1** contains unusual structural features that, while having precedent in other cyanobacterial natural products, have not previously been seen together. Terminal alkynes can be found in several other natural products from *Moorena* spp., including jamaicamide B [66], carmabin A [71], and vatiamides A, C, and E [72], but having two is notable. While ribosomally synthesized and post-translationally modified peptides (RiPPs) and NRPS-derived natural products with amino acid subunits are common in cyanobacteria, lysine is not often seen, especially in the natural products of marine cyanobacteria [73,74]. The heterocycle in **1**, composed of an acetate extended amino acid, has been observed in the malynгамides [65], jamaicamides [66], gallinamides [67], and other cyanobacterial natural products, but again, never has it been reported involving a lysine residue. Two curiosities of the biosynthesis of compound **1**, namely the origin of the two 2-methyl octynoic acid residues and the formation of the heterocycle, can be explained by analogy to what is known about the biosynthesis of the jamaicamides [66]. To generate 2-methyl octynoic acid, a fatty-acid desaturase analogous to Jamb could act upon an octanoic acid precursor, or a smaller precursor that has been PKS-extended to the appropriate size. The placement of the methyl group in the 2 position suggests incorporation via

S-adenosyl methionine (SAM). Formation of the heterocycle likely occurs as the result of an acetate extension of the carboxyl group of lysine, followed by a Claisen-like condensation and cyclization directed by a cyclase analogous to JamQ. As noted above in the discussion of structural possibilities 1a and 1b, what is less clear is how 2-methyl octynoic acid is appended to the terminus of the lysine side chain; the peptide bond formed is far from unusual, but its placement suggests enzymatic activity occurring beyond the otherwise linear PKS-NRPS assembly of the molecule.

To further evaluate the relationships of the structural features found together in compound 1 to the known natural product chemical space, we applied a Small Molecule Accurate Recognition Technology (SMART) [75] analysis to search for structurally similar molecules based on HSQC spectra. SMART did not yield any similar compounds with a cosine value higher than 0.84, further revealing the structural uniqueness of compound 1. We also utilized the structure similarity search function in SciFinder (<https://scifinder.cas.org/>), which yielded only the sintokamides (Figure S27). The sintokamides share a similar heterocycle and are halogenated natural products from sponges [76]. While not suggested by either structure similarity query, tetramic acids [77] and prostaglandins (PGE<sub>2</sub>, for example) [78] (Figure S27) are two chemical classes that possess some distant level of structural similarity to compound 1, and this inspired additional bioactivity testing efforts, as described below.

Structural similarity to tetramic acids inspired in silico antibiotic screening (<http://chemprop.csail.mit.edu/>) [79]. The known antibacterials C<sub>12</sub>-tetramic acid and C<sub>14</sub>-tetramic acid scored over five times greater than the highest scoring doscadenamide (Table S4), providing little incentive to further evaluate the doscadenamides for antibiotic activity.

Compound 1 was assayed for cytotoxicity against human NCI-H460 cells and yielded an IC<sub>50</sub> > 22 μM, suggesting negligible cytotoxicity. This lack of cytotoxicity, plus some distant structural similarity to prostaglandins, inspired the screening of compound 1 in a Griess assay for anti-inflammation (as well as cytotoxicity) toward murine macrophages RAW264.7 cells at a range of 7–55 μM. Curiously, rather than producing inflammatory or anti-inflammatory effects, compound 1 yielded dose-dependent synergistic cytotoxicity with lipopolysaccharide (LPS). This anomalous result was confirmed through multiple replicates of the assay (Figures S28–S30).

The doscadenamides were discovered based on global scale patterns in *M. bouillonii* chemical diversity. This illustrates that cyanobacteria harbor intraspecific chemogeographic patterns, and that these patterns can be utilized to direct discovery efforts towards new, regionally specific natural product families. There are many tools available for pursuing chemogeographic and other metabolite patterns in sample sets that can inform discovery efforts, each with their own strengths and limitations. While tools like the ORCA pipeline and GNPS classical molecular networking may be of limited utility in terms of quantitative analyses and effective separation of isomeric features, their flexibility in handling heterogeneous sample sets allows for comparative analyses between samples that could otherwise not be conducted. Furthermore, the intrinsic imperfection of real-world data and the deficiencies inherent to various tools and approaches encourages that an ensemble of tools and approaches be applied. By using ORCA in conjunction with GNPS, we were able to generate convergent results that increased confidence in our conclusions. Converging results from ORCA and GNPS were also helpful in giving confidence to the parameters selected for our analyses; parameter selection is often a challenge when applying computational techniques and requires deep knowledge of the dataset as well as manual validation. The chemogeographic patterns in *M. bouillonii* natural products that are qualitatively presented in this manuscript highlight the opportunity to further explore *M. bouillonii* natural products chemistry and how compounds and compound families are distributed ubiquitously vs. regionally, at different geographical scales. Studying *M. bouillonii* metabolomics in a more controlled, semi-quantitative fashion would allow these patterns to be evaluated more deeply and will be the focus of a future manuscript.

Doscadenamide A (1), when considered in isolation, is a structurally intriguing compound. Being composed of a heterocyclized, acetate-extended amino acid core appended with terminal alkyne containing side chains, it blends structural features common among cyanobacterial natural products

with a flair of the unusual: the inclusion of lysine, the dual terminal alkynes, and the acylation of the lysine side chain with one of those terminal alkyne containing side chains. In considering the doscadenamides as a family of cyanobacterial natural products, it is likely they are produced via a seemingly combinatorial addition of different acyl groups to a consistent core structure. From a biosynthetic perspective, this suggests a low level of fidelity in the assembly process. Connecting this family of compounds to the biosynthetic gene cluster responsible for their production would elevate our understanding of how cyanobacteria diversify their natural product arsenals. Since the aforementioned procedure for the total synthesis of compound **1** [29] is amenable to incorporating alternative sidechains, this could be used for generating the nine proposed natural structural analogs reported here (**2–10**), as well as for evaluating their activities as quorum sensing modulators [29] and their cytotoxic synergism with LPS.

### 3. Materials and Methods

#### 3.1. General Experimental Procedures

Optical rotation was measured using a JASCO P-2000 polarimeter (Easton, MD, USA), UV/Vis data were obtained using a Beckman DU800 spectrophotometer (Brea, CA, USA), and IR spectra were recorded on a ThermoScientific Nicolet 6700 FT-IR spectrometer (Waltham, MA, USA). NMR experiments were conducted using a JEOL ECZ 500 NMR spectrometer (Akishima, Tokyo, Japan) equipped with a 3 mm inverse probe (H3X), a Bruker AVANCE III 600 MHz NMR with a 1.7 mm dual tune TCI cryoprobe (Billerica, MA, USA), and a Varian VX500 (Palo Alto, CA, USA). NMR data were processed using Mestrenova (Mestrelab, Santiago de Compostela, Spain) and TopSpin (Bruker, Billerica, MA, USA). NMR data were recorded in CDCl<sub>3</sub> and referenced to the solvent peak (7.260, 77.160). For the low-resolution LC-MS/MS analysis, a ThermoFinnigan Surveyor HPLC System (San Jose, CA, USA) with a Phenomenex Kinetex 5 μm C18 100 × 4.6 mm column (Torrance, CA, USA) coupled to a ThermoFinnigan LCQ Advantage Max Mass Spectrometer (San Jose, CA, USA) in positive ion mode was used. Samples were analyzed using one of two linear gradients from 30% CH<sub>3</sub>CN + 0.1% formic acid to 99% CH<sub>3</sub>CN + 0.1% formic acid in H<sub>2</sub>O + 0.1% formic acid at a flow rate of either 0.6 mL/min or 0.7 mL/min over 32 min or 30 min, respectively. Samples were run at a concentration of 1 mg/mL, with concentrations increased up to 4 mg/mL in situations where the peak intensities were insufficient. For the HiRes-ESI-MS analysis, an Agilent 6230 time-of-flight mass spectrometer (TOFMS) (Santa Clara, CA, USA) with Jet Stream ESI source was used. For HiResMS<sup>2</sup> fragmentation data, a ThermoScientific Orbitrap XL mass spectrometer (Waltham, MA, USA) with direct infusion of the sample into the Thermo IonMax electrospray interface was used.

Compound isolation was performed using two semi-preparative HPLCs: a Thermo Scientific Dionex UltiMate 3000 HPLC (Waltham, MA, USA) system with automated fraction collector, a Waters HPLC system with 1500 series pumps (Milford, MA, USA), and a 996 photodiode array detector with manual fraction collection. HPLC separation was performed using a Phenomenex Kinetex 5 μm C18 10 × 150 mm column (Torrance, CA, USA) and reverse phase gradients of acetonitrile in H<sub>2</sub>O, with both solvents containing 0.1% (*v/v*) formic acid. HPLC grade organic solvents and Millipore Milli-Q system (Burlington, MA, USA) purified water were used.

All reagents, catalysts, and solvents used for the synthetic experiments were purchased in their purest and driest form. All experiments were carried out under an inert atmosphere (Ar) unless otherwise specified.

National Cancer Institute (NCI) H460 hypotriploid human cells [American Type Culture Collection (ATCC) HTB-177] and RAW 264.7 murine macrophages (ATCC TIB-71) were purchased from the ATCC (Manassas, VA, USA).

### 3.2. Sample Collection

Fifteen benthic filamentous tropical marine cyanobacterial samples were hand-collected via self-contained underwater breathing apparatus (SCUBA) or snorkeling in American Samoa, Guam, Kavaratti (Lakshadweep Islands, India), Papua New Guinea, Saipan, and the Paracel Islands (Xisha) in the South China Sea between the years 2005 and 2018. Samples from all locations besides Papua New Guinea were preserved in 1:1 seawater and either ethyl or isopropyl alcohol, transported back to laboratories, and stored frozen until extraction. The sample from Papua New Guinea was transported back to the laboratory in a culture flask and propagated in seawater (SW) BG-11 media [80]. For additional metadata about these samples, see Table S5.

### 3.3. Sample Preparation

Cyanobacterial biomass was exhaustively extracted with 2:1 dichloromethane and methanol, concentrated under vacuum, and resuspended in methanol or acetonitrile at a concentration of 1 mg/mL. Samples were prepared for LC-MS/MS analysis via elution through C18 solid phase extraction (SPE) cartridges.

### 3.4. ORCA Pipeline

Code, data files, and supporting documentation on use and workings of the ORCA pipeline are available at <https://github.com/c-leber/ORCA>, while the parameter sets used for the various analyses reported in this study are available in Tables S6–S8. ORCA was written in Python [81] and is built off the following Python packages: pandas (0.25.2) [82,83], numpy (1.16.5) [84,85], pyteomics (4.1.2) [86,87], scipy (1.3.1) [88], networkx (2.4) [89], matplotlib (3.0.3) [90], sklearn (0.21.3) [91], and seaborn (0.9.0) [92]. ORCA is available in the form of a Jupyter Notebook [93,94], to facilitate customization and interactive experimentation. Prior to analyses in ORCA, proprietary LC-MS datafiles were converted to mzXML using MSCONVERT (<https://bio.tools/msconvert>) [95], which is a part of the ProteoWizard Library [96]. MSCONVERT was also used to convert proprietary LC-MS/MS datafiles to mzML for the ORCA MS<sup>2</sup> Auxiliary pipeline, and to mzXML or mzML for GNPS.

### 3.5. GNPS Classical Molecular Networking

Molecular networks were created using the online workflow (<https://ccms-ucsd.github.io/GNPSDocumentation/>) on the GNPS website (<http://gnps.ucsd.edu>) and were visualized using Cytoscape (3.7.2) (<https://cytoscape.org/>) [97] and the GNPS in-browser network visualizer. For full accounting of the networking parameter sets, see Tables S9–S11.

### 3.6. Compound Isolation

*M. bouillonii* biomass from Laulau Bay, Saipan, was thoroughly extracted with 2:1 dichloromethane and methanol, yielding 10 g crude extract from 132 g (1 L) biomass. A portion of the crude extract was fractionated over silica with vacuum liquid chromatography and a standardized solvent system protocol (Table S12). Two relatively polar fractions (fractions F and G) were found to contain the bulk of compound **1**. Reverse phase HPLC was used to isolate 2.6 mg of this compound from these two fractions. A gradient method from 37% to 50% CH<sub>3</sub>CN + 0.1% formic acid in H<sub>2</sub>O + 0.1% formic acid over 60 min at a flow rate of 4 mL/min resulted in the elution of compound **1** starting at a retention time of approximately 38 min.

### 3.7. Planar Structure Characterization

Compound **1**: white solid,  $[\alpha]_D^{26} +17.7$  (c 0.1, MeOH); UV/Vis (Figure S31); IR (Figure S32). NMR data Table S13; <sup>1</sup>H, <sup>13</sup>C, COSY, HSQC, HMBC, HSQC-TOCSY, and long-range HSQMBC spectra (Figures S33–S39); HR ESIMS (observed *m/z* [M + Na]<sup>+</sup> at 479.2877, C<sub>27</sub>H<sub>40</sub>N<sub>2</sub>O<sub>4</sub>, calculated 479.2880).



### 3.8. Structure Elucidation—Standard Preparation and Derivatization for Configurational Characterization

Methods for ZACA methylalumination-oxidation [68], catalytic hydrogenation [98], ozonolysis [69,99], acid hydrolysis [69,98,99], peptide coupling [98,100], and derivatization with Marfey's reagent [98,99] were adapted from the literature.

#### 3.8.1. Synthesis of (S)-2-methyloctanoic Acid

To a solution of trimethylaluminum (891  $\mu$ L, 1.782 mmol) and (+)-(NMI)<sub>2</sub>ZrCl<sub>2</sub> (23.84 mg, 0.036 mmol) in 1.5 mL of CH<sub>2</sub>Cl<sub>2</sub> was added a solution of oct-1-ene (100 mg, 0.891 mmol) in 1.5 mL of CH<sub>2</sub>Cl<sub>2</sub>. After stirring overnight at 23 °C, the mixture was treated with a vigorous stream of O<sub>2</sub> for 1 h at 0 °C and then stirred for 5 h under an atmosphere of O<sub>2</sub> at room temperature. The reaction mixture was quenched with 1 M HCl, extracted with CH<sub>2</sub>Cl<sub>2</sub>, washed with brine, dried over MgSO<sub>4</sub> and concentrated. The residue was purified via silica flash column chromatography (20% ethyl acetate/hexanes) to yield (S)-2-methyloctan-1-ol (50 mg, 0.347 mmol, 39% yield) as a clear oil. The crude product was used in the next step without further purification.

To a solution of (S)-2-methyloctan-1-ol (50 mg, 0.347 mmol) in acetonitrile (1.4 mL) was added *N*-methyl morpholine *N*-oxide (NMO) solution in H<sub>2</sub>O (468 mg, 3.47 mmol) and tetrapropylammonium perruthenate (TPAP) (12.18 mg, 0.035 mmol) sequentially at room temperature and the mixture was stirred for 2 h. The mixture was then concentrated, and the residue passed through a pad of silica gel using hexanes:diethyl ether (3:1) containing 0.1% acetic acid. The eluted solvent was concentrated to yield (S)-2-methyloctanoic acid (48 mg, 0.303 mmol, 88% yield).  $[\alpha]_D^{26} +10.0$  (c 1.05, MeOH); <sup>1</sup>H NMR (500 MHz, CDCl<sub>3</sub>)  $\delta$  2.46 (ddq, J = 9.7, 6.8, 3.1 Hz, 1H), 1.69 (m, 2H), 1.44 (m, 2H), 1.37–1.24 (m, 6H), 1.19 (m, 3H), 0.89 (m, 3H); <sup>13</sup>C NMR (126 MHz, CDCl<sub>3</sub>)  $\delta$  183.2, 39.6, 33.7, 31.9, 29.4, 27.3, 22.8, 17.1, 14.3. HRESIMS *m/z* [M + H]<sup>+</sup> 159.1394 (calc. for C<sub>9</sub>H<sub>19</sub>O<sub>2</sub>, 159.1385).

#### 3.8.2. Derivatization of 2-methyloctanoic Acid with 2-phenylglycine Methyl Ester

To generate a 1:1 standard mixture of both possible diastereomers of 2-methyloctanoic acid, 6.0 mg (37.9  $\mu$ mol) of racemic 2-methyloctanoic acid was combined with 1-[bis(dimethylamino)methylene]-1H-1,2,3-triazolo[4,5-b]pyridinium 3-oxid hexafluorophosphate (HATU) (14.4 mg, 37.9  $\mu$ mol), (S)-(+)-2-phenylglycine methyl ester hydrochloride (7.6 mg, 37.9  $\mu$ mol) and *N,N*-diisopropylethylamine (DIPEA) (30  $\mu$ L) in dimethylformamide (DMF) (300  $\mu$ L). This was stirred overnight at room temperature and ambient atmosphere. The reaction mixture was then diluted with 1.0 mL of EtOAc, washed with saturated aqueous NH<sub>4</sub>Cl (3  $\times$  1.0 mL), concentrated under vacuum, and prepared for LC-MS analysis. To generate a chiral standard, 1.8 mg (11.4  $\mu$ mol) of (S)-2-methyloctanoic acid was combined with HATU (4.3 mg, 11.4  $\mu$ mol), (S)-(+)-2-phenylglycine methyl ester hydrochloride (2.3 mg, 11.4  $\mu$ mol) and DIPEA (30  $\mu$ L) in DMF (300  $\mu$ L), and stirred overnight at room temperature and ambient atmosphere. The reaction mixture was then diluted with 1.0 mL of EtOAc, washed with saturated aqueous NH<sub>4</sub>Cl (3  $\times$  1.0 mL), concentrated under vacuum, and prepared for LC-MS analysis. The diastereomeric ratio of the chiral standard was 3:1 by area-under-curve analysis.

#### 3.8.3. Derivatization of Lysine with Marfey's Reagent (FDAA)

To generate a racemic standard, 0.8 mg (4  $\mu$ mol) of racemic lysine hydrochloride and 0.1 M NaHCO<sub>3</sub> (200  $\mu$ L) were added to a solution of L-FDAA (4.4 mg, 16  $\mu$ mol) in acetone (600  $\mu$ L). The reaction mixture was sealed in a vial with ambient atmosphere, stirred at 90 °C for 5 min, neutralized with 6 M HCl, concentrated under vacuum, and prepared for LC-MS analysis. To generate a chiral standard, 1.0 mg (6  $\mu$ mol) of L-lysine monohydrate and 0.1 M NaHCO<sub>3</sub> (200  $\mu$ L) were added to a solution of L-FDAA (6.5 mg, 24  $\mu$ mol) in acetone (600  $\mu$ L). The reaction mixture was sealed in a vial with ambient atmosphere, stirred at 90 °C for 5 min, neutralized with 6 M HCl, concentrated under vacuum, and prepared for LC-MS analysis.

### 3.8.4. Derivatization of Compound 1

Compound 1 (0.5 mg) was combined with 1.0 mg of Pd/C in 1 mL EtOH and stirred under an atmosphere of H<sub>2</sub> for 8 h. The mixture was filtered through glass wool, rinsed with EtOH (3 × 1.0 mL), and concentrated in vacuo.

Hydrogenated compound 1 (0.25 mg) was dissolved in 1 mL CH<sub>2</sub>Cl<sub>2</sub>, into which a stream of ozone gas was bubbled at −78 °C for 25 min. The reaction was concentrated under vacuum, and the residue was treated with 1 mL of 1:2 35% H<sub>2</sub>O<sub>2</sub>:HCOOH at 70 °C and ambient atmosphere for 20 min. The reaction was again concentrated in vacuo, followed by the addition of 1 mL 6 M HCl. The reaction mixture was stirred in a sealed vial with ambient atmosphere overnight at 110 °C, and then concentrated under vacuum. To the residue, a solution of L-FDAA (0.6 mg, 2 μmol) in acetone (200 μL) and 0.1 M NaHCO<sub>3</sub> (200 μL) were added. The reaction mixture was sealed in a vial with ambient atmosphere, stirred at 90 °C for 5 min, neutralized with 6 M HCl, concentrated in vacuo, and prepared for LC-MS analysis.

Hydrogenated compound 1 (0.25 mg) was dissolved in 1 mL 6 M HCl. This reaction mixture was stirred in a sealed vial with ambient atmosphere overnight at 110 °C, and then concentrated under vacuum. The residue was combined with HATU (0.4 mg, 1 μmol), (S)-(+)-2-phenylglycine methyl ester hydrochloride (0.2 mg, 1 μmol), and DIPEA (20 μL) in DMF (200 μL) and stirred for 6 h at room temperature and at ambient atmosphere. The reaction mixture was then diluted with 1.0 mL of EtOAc, washed with saturated aqueous NH<sub>4</sub>Cl (3 × 1.0 mL), concentrated under vacuum, and prepared for LC-MS analysis.

### 3.9. ORCA MS<sup>2</sup> Auxiliary Pipeline

Code, data files, and supporting documentation on the use and workings of the ORCA MS<sup>2</sup> Auxiliary pipeline are available at <https://github.com/c-leber/ORCA>. MS<sup>2</sup> spectra were binned with the bin\_OOM parameter set to 0, and the cutoff parameter for the hierarchical clustering of the MS<sup>2</sup> scans for a particular precursor mass was set to 0.15. The MS<sup>2</sup> scans were filtered to only include scans for precursor masses, which contained fragment peaks with *m/z* 168, resulting in 78 precursor masses. These precursor masses were individually analyzed via the hierarchical clustering of scan fragmentation patterns followed by the generation of consensus spectra for each cluster. Consensus spectra were manually inspected to detect interpretable fragmentation patterns similar to those of compound 1.

### 3.10. Bioassays

Methods for the NCI-H460 cytotoxicity assay [101] and the Griess assay [102,103] were adapted from the literature.

#### 3.10.1. Cytotoxicity Assay of Compound 1 with NCI-H460 Cell Line

NCI-H460 hypotriploid human cells (ATCC HTB-177) were grown in monolayers to near confluence in flasks and then seeded into wells at  $3.33 \times 10^4$  cells/mL of Roswell Park Memorial Institute (RPMI) medium with standard fetal bovine serum (FBS), 180 μL/well, and incubated for 24 h at 37 °C in 96-well plates. Cells were exposed to compound 1 at ten half log concentrations, the highest being 21.9 μM with 1% dimethyl sulfoxide (DMSO) present, while the lowest was 0.7 nM. Plates were incubated for an additional 48 h and then stained with 3-(4,5-dimethylthiazol-2-yl)-2,5-diphenyltetrazolium bromide (MTT), for 25 min, after which the optical densities were recorded at 630 and 570 nm for each well on a SpectraMax M2 microplate reader with SoftMax<sup>®</sup> Pro Microplate Data Acquisition and Analysis Software (Molecular Devices, LLC, Version No. M2, Sunnyvale, CA, USA). The test samples were compared with a negative control of 1% DMSO and a positive control of doxorubicin (0.1 μg/mL and 1 μg/mL), both in RPMI medium. Due to the limited availability of compound 1, fully toxic concentrations were not reached; hence, the resultant dose–response curve was incomplete. Nevertheless, the IC<sub>50</sub> value for compound 1 is greater than 21.9 μM.

### 3.10.2. Griess Assay and Cytotoxicity of Compound 1 in RAW 264.7 Cells

RAW 264.7 murine macrophages (ATCC TIB-71) were seeded at  $5 \times 10^4$  cells in 96-well plates in Dulbecco's Modified Eagle Medium (DMEM; Gibco, Carlsbad, CA, USA) supplemented with 10% endotoxin-low FBS (HyClone, characterized, Endotoxin:  $\leq 25$  EU/mL), 190  $\mu$ L/well, and incubated for 24 h at 37 °C. Compound 1 at concentrations of 55, 28, 14, or 7  $\mu$ M was applied in triplicate, and after 1 h lipopolysaccharide (LPS from *Escherichia coli* 026:B6, =10,000 EU/mg, Sigma-Aldrich, Oakville, ON, Canada) was added (0.5 or 1.5  $\mu$ g/mL) to all wells except those for the LPS-free controls and those for evaluating the pro-inflammatory effects of compound 1. LPS alone was used as a negative control, whereas the same LPS concentration with 1% DMSO served as the positive control in the Griess assay. After 24 h, Griess reactions (Section 3.10.3) were used to assess NO generation as a proxy for inflammation, and MTT staining (Section 3.10.1) was used to assess cell viability. Doxorubicin at 3.3  $\mu$ g/mL was used as a positive control for assessing cell viability. Cell survival was calculated as a percentage compared to wells with 1% or 1.5% EtOH and no LPS. A NO concentration standard curve was prepared in Microsoft Excel based on eight serial dilutions of a nitrite standard (0–100  $\mu$ M) with DMEM. One-way ANOVA and Tukey's method were used to test for significance in the cell survival results from the assay; high mortality in certain conditions made statistical analyses of the inflammation data inappropriate. Statistical analyses were applied using GraphPad Prism version 8.0.0 for Windows. Batch variability in LPS potency and RAW 264.7 murine macrophage sensitivity, as well as limited availability of compound 1 necessitated using differing reagent concentrations across the biological replicates.

### 3.10.3. Griess Reaction

Supernatant from each sample well (50  $\mu$ L) was added to the experimental wells in triplicate. A 1:1 mixture of 1% sulfanilamide solution in 5% phosphoric acid and 0.1% *N*-1-naphthylethylenediamine dihydrochloride (100  $\mu$ L) was added to each well and the plate was incubated in the dark for 20 min. Optical density was measured at 570 nm on a SpectraMax M2 microplate reader. The raw data were exported to a Microsoft Excel work sheet and the concentration of nitrite in the samples was determined by comparison to the standard curve using regression analysis.

### 3.10.4. In silico Antibiotic Screening

The simplified molecular-input line-entry system (SMILES) structures of compound 1, proposed analogs 2–10, C<sub>12</sub>-tertramric acid, and C<sub>14</sub>-tetramric acid were submitted to Chemprop Predict (<http://chemprop.csail.mit.edu/predict>) [79], using the Antibiotics model checkpoint.

**Supplementary Materials:** The following are available online at <http://www.mdpi.com/1660-3397/18/10/515/s1>, Figure S1: Molecular network of *M. bouillonii* crude extracts; Figure S2: Predicted <sup>13</sup>C shifts for candidate structure 1a; Figure S3: Predicted <sup>13</sup>C shifts for candidate structure 1b; Figure S4: Compound 1 derived 2-methyloctanoic acid compared to standards; Figure S5: Compound 1 derived lysine compared to standards; Figure S6: Doscadenamide A (1) consensus MS<sup>2</sup> spectrum; Figure S7: Molecular network cluster of compound 1 and analogs, highlighting *m/z* 168 frag. peak; Figure S8: Structure of compound 1 with structure proposals for analogs (2–10); Figure S9: Doscadenamide B (2) consensus MS<sup>2</sup> spectrum; Figure S10: Doscadenamide B (2) proposed fragmentation; Figure S11: Doscadenamide C (3) consensus MS<sup>2</sup> spectrum; Figure S12: Doscadenamide C (3) proposed fragmentation; Figure S13: Doscadenamide D (4) consensus MS<sup>2</sup> spectrum; Figure S14: Doscadenamide D (4) proposed fragmentation; Figure S15: Doscadenamide E (5) consensus MS<sup>2</sup> spectrum; Figure S16: Doscadenamide E (5) proposed fragmentation; Figure S17: Doscadenamide F (6) consensus MS<sup>2</sup> spectrum; Figure S18: Doscadenamide F (6) proposed fragmentation; Figure S19: Doscadenamide G (7) consensus MS<sup>2</sup> spectrum; Figure S20: Doscadenamide G (7) proposed fragmentation; Figure S21: Doscadenamide H (8) consensus MS<sup>2</sup> spectrum; Figure S22: Doscadenamide H (8) proposed fragmentation; Figure S23: Doscadenamide I (9) consensus MS<sup>2</sup> spectrum; Figure S24: Doscadenamide I (9) proposed fragmentation; Figure S25: Doscadenamide J (10) consensus MS<sup>2</sup> spectrum; Figure S26: Doscadenamide J (10) proposed fragmentation; Figure S27: Representative structures from compound families similar to the doscadenamides; Figure S28: Results of compound 1 in Griess assay—biological replicate 1; Figure S29: Results of compound 1 in Griess assay—biological replicate 2; Figure S30: Results of compound 1 in Griess assay—biological replicate 3; Figure S31: UV/Vis absorbance spectrum (200–400 nm) for compound 1; Figure S32: IR spectrum for compound 1; Figure S33: <sup>1</sup>H NMR spectrum for

compound **1**; Figure S34:  $^{13}\text{C}$  NMR spectrum for compound **1**; Figure S35:  $^1\text{H}$ - $^1\text{H}$  COSY spectrum for compound **1**; Figure S36:  $^1\text{H}$ - $^{13}\text{C}$  HSQC spectrum for compound **1**; Figure S37:  $^1\text{H}$ - $^{13}\text{C}$  HMBC spectrum for compound **1**; Figure S38:  $^1\text{H}$ - $^{13}\text{C}$  HSQC-TOCSY spectrum for compound **1**; Figure S39:  $^1\text{H}$ - $^{13}\text{C}$  Long-range HSQMBC spectrum for compound **1**; Table S1: Known compounds isolated from *M. bouillonii*; Table S2: Average relative abundances and feature selection scores for top 10 Saipan MS<sup>1</sup> features; Table S3: Putative identifications for top 30 MS<sup>1</sup> features in the *M. bouillonii* crude extract dataset; Table S4: In silico antibiotic screening results for the doscadenamides and tetramic acids; Table S5: *M. bouillonii* crude extract sample metadata; Table S6: ORCA parameter set for MS<sup>1</sup> feature dendrogram; Table S7: ORCA parameter set for GNPS MS<sup>2</sup> feature presence/absence dendrogram; Table S8: ORCA parameter set for MS<sup>1</sup> feature selection; Table S9: GNPS parameter set for *M. bouillonii* crude extract molecular network; Table S10: GNPS parameter set for *M. bouillonii* crude extract MS<sup>2</sup> feature bucket table; Table S11: GNPS parameter set for Saipan and Guam crude extracts and fractions molecular network; Table S12: VLC fractionation solvent systems; and Table S13:  $^1\text{H}$  and  $^{13}\text{C}$  NMR data for doscadenamide A (**1**) in CDCl<sub>3</sub>.

**Author Contributions:** Conceptualization, C.A.L. and W.H.G.; methodology, C.A.L., C.B.N., L.K., J.A. and E.J.E.C.-D.; software, C.A.L.; validation, C.A.L.; formal analysis, C.A.L.; investigation, C.A.L., C.B.N., L.K., J.A., E.J.E.C.-D. and E.G.; resources, C.A.L., C.B.N., J.A., E.J.E.C.-D., E.G., V.J., T.P.S., A.J.R., J.S.B., T.L., Y.Y., S.H., X.Y. and W.H.G.; data curation, C.A.L.; writing—original draft preparation, C.A.L. and W.H.G.; writing—review and editing, C.A.L., C.B.N., L.K., J.A., E.J.E.C.-D., E.G., V.J., T.P.S., A.J.R., J.S.B., T.L., Y.Y., S.H., X.Y. and W.H.G.; visualization, C.A.L.; supervision, W.H.G.; project administration, C.A.L.; funding acquisition, W.H.G. and C.B.N. All authors have read and agreed to the published version of the manuscript.

**Funding:** This study was supported by the National Institutes of Health (NIH) (grant GM107550 to W.H.G.) and the Gordon and Betty Moore Foundation (grant GBMF7622 to W.H.G.). This study was further supported in part by the National Key Research and Development Program of China, funded through MOST (the Ministry of Science and Technology of China; grant 2018YFC0310900 to X.Y. and C.B.N.), NSFC (the National Natural Science Foundation of China; grant 81850410553 to C.B.N.), and Ningbo STI (Ningbo Science and Technology Bureau; grant 010-20171JCGY01172 to C.B.N.). A portion of this study was supported by the University Grants Commission, Government of India under Indo-US 21st Century Knowledge Initiative Project (Grant No. 194-1/2009(IC) dated 7/2/2015) to V.J. and T.P.S. C.A.L. was supported by the UCSD Regents Pre-Doctoral Fellowship, the Robert L. Cody Memorial Pre-Doctoral Fellowship, the Kaplan Trust CMBB Pre-Doctoral Fellowship, and the NIH Training Program in Marine Biotechnology (T32GM067550). L.K. was supported by the Deutsche Forschungsgemeinschaft (Grant KE 2172/3-1 and KE 2172/4-1).

**Acknowledgments:** We acknowledge F.M. Brunner and C.P. Kubiak (UCSD Department of Chemistry & Biochemistry) for facilitating acquisition of IR data, and Y. Su, and L. Gross for HiRes mass spectrometry support at the UCSD Molecular Mass Spectrometry Facility. We thank B. Duggan and A. Mrse for NMR support, and M.P. Christy (Scripps Institution of Oceanography, UCSD) for support with the synthesis of standards. We also acknowledge the government of Sansha city, China, for permission to collect and study several of the marine samples used in this research and the sample collection assistance from L. Zhenhua, L. Daning and H. Da of the Xisha Marine Science Comprehensive Experimental Station, South China Sea Institute of Oceanology, Chinese Academy of Sciences. We acknowledge the support of I.S. Bright Singh of the National Centre for Aquatic Animal Health, Cochin University of Science and Technology, India, and the Department of Science and Technology, Kavarratti, Lakshadweep Islands, India for the required research permits. C.L. acknowledges travel support from the LBG foundation.

**Conflicts of Interest:** William H. Gerwick declares a competing financial interest as a cofounder of NMR Finder LLC. Otherwise, the authors declare no conflict of interest. The funders had no role in the design of the study; in the collection, analyses, or interpretation of data; in the writing of the manuscript, or in the decision to publish the results.

## References

1. Chanana, S.; Thomas, C.S.; Braun, D.R.; Hou, Y.; Wyche, T.P.; Bugni, T.S. Natural Product Discovery Using Planes of Principal Component Analysis in R (PoPCAR). *Metabolites* **2017**, *7*, 34. [[CrossRef](#)]
2. Clark, C.M.; Costa, M.S.; Sanchez, L.M.; Murphy, B.T. Coupling MALDI-TOF mass spectrometry protein and specialized metabolite analyses to rapidly discriminate bacterial function. *Proc. Natl. Acad. Sci. USA* **2018**, *115*, 4981–4986. [[CrossRef](#)]
3. Wang, M.; Carver, J.J.; Phelan, V.V.; Sanchez, L.M.; Garg, N.; Peng, Y.; Nguyen, D.D.; Watrous, J.; Kapon, C.A.; Luzzatto-Knaan, T.; et al. Sharing and community curation of mass spectrometry data with Global Natural Products Social Molecular Networking. *Nat. Biotechnol.* **2016**, *34*, 828–837. [[CrossRef](#)]
4. Nothias, L.F.; Petras, D.; Schmid, R.; Dührkop, K.; Rainer, J.; Sarvepalli, A.; Protsyuk, I.; Ernst, M.; Tsugawa, H.; Fleischauer, M.; et al. Feature-based Molecular Networking in the GNPS Analysis Environment. *Nat. Methods* **2020**, *17*, 905–908. [[CrossRef](#)]

5. Gowda, H.; Ivanisevic, J.; Johnson, C.H.; Kurczy, M.E.; Benton, H.P.; Rinehart, D.; Nguyen, T.; Ray, J.; Kuehl, J.; Arevalo, B.; et al. Interactive XCMS Online: Simplifying Advanced Metabolomic Data Processing and Subsequent Statistical Analyses. *Anal. Chem.* **2014**, *86*, 6931–6939. [[CrossRef](#)] [[PubMed](#)]
6. Pluskal, T.; Castillo, S.; Villar-Briones, A.; Orešič, M. MZmine 2: Modular framework for processing, visualizing, and analyzing mass spectrometry-based molecular profile data. *BMC Bioinform.* **2010**, *11*, 395. [[CrossRef](#)] [[PubMed](#)]
7. Chong, J.; Soufan, O.; Li, C.; Caraus, I.; Li, S.; Bourque, G.; Wishart, D.S.; Xia, J. MetaboAnalyst 4.0: Towards more transparent and integrative metabolomics analysis. *Nucleic Acids Res.* **2018**, *46*, W486–W494. [[CrossRef](#)] [[PubMed](#)]
8. Tronholm, A.; Engene, N. *Moorea* gen. nov., a valid name for “*Moorea Engene & al.*” nom. inval. (Oscillatoriaceae, Cyanobacteria). *Notulae Algarum* **2019**, *122*, 1–2.
9. Engene, N.; Rottacker, E.C.; Kaštovský, J.; Byrum, T.; Choi, H.; Ellisman, M.H.; Komárek, J.; Gerwick, W.H. *Moorea producens* gen. nov., sp. nov. and *Moorea bouillonii* comb. nov., tropical marine cyanobacteria rich in bioactive secondary metabolites. *Int. J. Syst. Evol. Micr.* **2012**, *62*, 1171–1178. [[CrossRef](#)] [[PubMed](#)]
10. Leao, T.; Castelão, G.; Korobeynikov, A.; Monroe, E.A.; Podell, S.; Glukhov, E.; Allen, E.E.; Gerwick, W.H.; Gerwick, L. Comparative genomics uncovers the prolific and distinctive metabolic potential of the cyanobacterial genus *Moorea*. *Proc. Natl. Acad. Sci. USA* **2017**, *114*, 3198–3203. [[CrossRef](#)] [[PubMed](#)]
11. Williams, P.G.; Luesch, H.; Yoshida, W.Y.; Moore, R.E.; Paul, V.J. Continuing Studies on the Cyanobacterium *Lyngbya* sp.: Isolation and Structure Determination of 15-Norlyngbyapeptin A and Lyngbyabellin D. *J. Nat. Prod.* **2003**, *66*, 595–598. [[CrossRef](#)]
12. Matthew, S.; Salvador, L.A.; Schupp, P.J.; Paul, V.J.; Luesch, H. Cytotoxic Halogenated Macrolides and Modified Peptides from the Apratoxin-Producing Marine Cyanobacterium *Lyngbya bouillonii* from Guam. *J. Nat. Prod.* **2010**, *73*, 1544–1552. [[CrossRef](#)]
13. Choi, H.; Mevers, E.; Byrum, T.; Valeriote, F.A.; Gerwick, W.H. Lyngbyabellins K–N from two Palmyra atoll collections of the marine cyanobacterium *Moorea bouillonii*. *Eur. J. Org. Chem.* **2012**, *2012*, 5141–5150. [[CrossRef](#)]
14. Soria-Mercado, I.E.; Pereira, A.; Cao, Z.; Murray, T.F.; Gerwick, W.H. Alotamide A, a novel neuropharmacological agent from the marine cyanobacterium *Lyngbya bouillonii*. *Org. Lett.* **2009**, *11*, 4704–4707. [[CrossRef](#)]
15. Luesch, H.; Yoshida, W.Y.; Moore, R.E.; Paul, V.J. Apramides A–G, Novel Lipopeptides from the Marine Cyanobacterium *Lyngbya majuscula*. *J. Nat. Prod.* **2000**, *63*, 1106–1112. [[CrossRef](#)]
16. Luesch, H.; Yoshida, W.Y.; Moore, R.E.; Paul, V.J.; Corbett, T.H. Total Structure Determination of Apratoxin A, a Potent Novel Cytotoxin from the Marine Cyanobacterium *Lyngbya majuscula*. *J. Am. Chem. Soc.* **2001**, *123*, 5418–5423. [[CrossRef](#)]
17. Thornburg, C.C.; Cowley, E.S.; Sikorska, J.; Shaala, L.A.; Ishmael, J.E.; Youssef, D.T.A.; McPhail, K.L. Apratoxin H and Apratoxin A Sulfoxide from the Red Sea Cyanobacterium *Moorea producens*. *J. Nat. Prod.* **2013**, *76*, 1781–1788. [[CrossRef](#)]
18. Luesch, H.; Yoshida, W.Y.; Moore, R.E.; Paul, V.J. New apratoxins of marine cyanobacterial origin from guam and palau. *Bioorg. Med. Chem.* **2002**, *10*, 1973–1978. [[CrossRef](#)]
19. Gutiérrez, M.; Suyama, T.L.; Engene, N.; Wingerd, J.S.; Matainaho, T.; Gerwick, W.H. Apratoxin D, a Potent Cytotoxic Cyclodepsipeptide from Papua New Guinea Collections of the Marine Cyanobacteria *Lyngbya majuscula* and *Lyngbya sordida*. *J. Nat. Prod.* **2008**, *71*, 1099–1103. [[CrossRef](#)]
20. Matthew, S.; Schupp, P.J.; Luesch, H. Apratoxin E, a Cytotoxic Peptolide from a Guamanian Collection of the Marine Cyanobacterium *Lyngbya bouillonii*. *J. Nat. Prod.* **2008**, *71*, 1113–1116. [[CrossRef](#)]
21. Tidgewell, K.; Engene, N.; Byrum, T.; Media, J.; Doi, T.; Valeriote, F.A.; Gerwick, W.H. Evolved Diversification of a Modular Natural Product Pathway: Apratoxins F and G, Two Cytotoxic Cyclic Depsipeptides from a Palmyra Collection of *Lyngbya bouillonii*. *Chembiochem* **2010**, *11*, 1458–1466. [[CrossRef](#)] [[PubMed](#)]
22. Cai, W.; Salvador-Reyes, L.A.; Zhang, W.; Chen, Q.Y.; Matthew, S.; Ratnayake, R.; Seo, S.J.; Dolles, S.; Gibson, D.J.; Paul, V.J.; et al. Apratyramide, a Marine-Derived Peptidic Stimulator of VEGF-A and Other Growth Factors with Potential Application in Wound Healing. *ACS Chem. Biol.* **2018**, *13*, 91–99. [[CrossRef](#)]
23. Tan, L.T.; Okino, T.; Gerwick, W.H. Bouillonamide: A Mixed Polyketide-Peptide Cytotoxin from the Marine Cyanobacterium *Moorea bouillonii*. *Mar. Drugs* **2013**, *11*, 3015–3024. [[CrossRef](#)] [[PubMed](#)]

24. Rubio, B.K.; Parrish, S.M.; Yoshida, W.; Schupp, P.J.; Schils, T.; Williams, P.G. Depsipeptides from a Guamanian marine cyanobacterium, *Lyngbya bouillonii*, with selective inhibition of serine proteases. *Tetrahedron Lett.* **2010**, *51*, 6718–6721. [[CrossRef](#)]
25. Kleigrewe, K.; Almaliti, J.; Tian, I.Y.; Kinnel, R.B.; Korobeynikov, A.; Monroe, E.A.; Duggan, B.M.; Di Marzo, V.; Sherman, D.H.; Dorrestein, P.C.; et al. Combining Mass Spectrometric Metabolic Profiling with Genomic Analysis: A Powerful Approach for Discovering Natural Products from Cyanobacteria. *J. Nat. Prod.* **2015**, *78*, 1671–1682. [[CrossRef](#)]
26. Lopez, J.A.V.; Petitbois, J.G.; Vairappan, C.S.; Umezawa, T.; Matsuda, F.; Okino, T. Columbamides D and E: Chlorinated Fatty Acid Amides from the Marine Cyanobacterium *Moorea bouillonii* Collected in Malaysia. *Org. Lett.* **2017**, *19*, 4231–4234. [[CrossRef](#)]
27. Mehjabin, J.J.; Wei, L.; Petitbois, J.G.; Umezawa, T.; Matsuda, F.; Vairappan, C.S.; Morikawa, M.; Okino, T. Biosurfactants from Marine Cyanobacteria Collected in Sabah, Malaysia. *J. Nat. Prod.* **2020**, *83*, 1925–1930. [[CrossRef](#)]
28. Pereira, A.R.; McCue, C.F.; Gerwick, W.H. Cyanolide A, a Glycosidic Macrolide with Potent Molluscicidal Activity from the Papua New Guinea Cyanobacterium *Lyngbya bouillonii*. *J. Nat. Prod.* **2010**, *73*, 217–220. [[CrossRef](#)]
29. Liang, X.; Matthew, S.; Chen, Q.Y.; Kwan, J.C.; Paul, V.J.; Luesch, H. Discovery and Total Synthesis of Doscadenamide A: A Quorum Sensing Signaling Molecule from a Marine Cyanobacterium. *Org. Lett.* **2019**, *21*, 7274–7278. [[CrossRef](#)] [[PubMed](#)]
30. Nakamura, F.; Maejima, H.; Kawamura, M.; Arai, D.; Okino, T.; Zhao, M.; Ye, T.; Lee, J.; Chang, Y.; Fusetani, N.; et al. Kakeromamide A, a new cyclic pentapeptide inducing astrocyte differentiation isolated from the marine cyanobacterium *Moorea bouillonii*. *Bioorg. Med. Chem. Lett.* **2018**, *28*, 2206–2209. [[CrossRef](#)]
31. Sweeney-Jones, A.M.; Gagaring, K.; Antonova-Koch, J.; Zhou, H.; Mojib, N.; Soapi, K.; Skolnick, J.; McNamara, C.W.; Kubanek, J. Antimalarial Peptide and Polyketide Natural Products from the Fijian Marine Cyanobacterium *Moorea producens*. *Mar. Drugs* **2020**, *18*, 167. [[CrossRef](#)]
32. Sumimoto, S.; Iwasaki, A.; Ohno, O.; Sueyoshi, K.; Teruya, T.; Suenaga, K. Kanamienamide, an Enamide with an Enol Ether from the Marine Cyanobacterium *Moorea bouillonii*. *Org. Lett.* **2016**, *18*, 4884–4887. [[CrossRef](#)]
33. Klein, D.; Braekman, J.C.; Daloze, D.; Hoffmann, L.; Demoulin, V. Laingolide, a novel 15-membered macrolide from *Lyngbya bouillonii* (cyanophyceae). *Tetrahedron Lett.* **1996**, *37*, 7519–7520. [[CrossRef](#)]
34. Klein, D.; Braekman, J.C.; Daloze, D.; Hoffmann, L.; Castillo, G.; Demoulin, V. Madangolide and Laingolide A, Two Novel Macrolides from *Lyngbya bouillonii* (Cyanobacteria). *J. Nat. Prod.* **1999**, *62*, 934–936. [[CrossRef](#)]
35. Tan, L.T.; Márquez, B.L.; Gerwick, W.H. Lyngbouilloside, a Novel Glycosidic Macrolide from the Marine Cyanobacterium *Lyngbya bouillonii*. *J. Nat. Prod.* **2002**, *65*, 925–928. [[CrossRef](#)]
36. Luesch, H.; Yoshida, W.Y.; Moore, R.E.; Paul, V.J.; Mooberry, S.L. Isolation, Structure Determination, and Biological Activity of Lyngbyabellin A from the Marine Cyanobacterium *Lyngbya majuscula*. *J. Nat. Prod.* **2000**, *63*, 611–615. [[CrossRef](#)]
37. Luesch, H.; Yoshida, W.Y.; Moore, R.E.; Paul, V.J. Isolation and Structure of the Cytotoxin Lyngbyabellin B and Absolute Configuration of Lyngbyapeptin A from the Marine Cyanobacterium *Lyngbya majuscula*. *J. Nat. Prod.* **2000**, *63*, 1437–1439. [[CrossRef](#)]
38. Luesch, H.; Yoshida, W.Y.; Moore, R.E.; Paul, V.J. Structurally diverse new alkaloids from Palauan collections of the apratoxin-producing marine cyanobacterium *Lyngbya* sp. *Tetrahedron* **2002**, *58*, 7959–7966. [[CrossRef](#)]
39. Klein, D.; Braekman, J.C.; Daloze, D.; Hoffmann, L.; Demoulin, V. Lyngbyaloside, a Novel 2,3,4-Tri-O-methyl-6-deoxy- $\alpha$ -mannopyranoside Macrolide from *Lyngbya bouillonii* (Cyanobacteria). *J. Nat. Prod.* **1997**, *60*, 1057–1059. [[CrossRef](#)]
40. Luesch, H.; Yoshida, W.Y.; Harrigan, G.G.; Doom, J.P.; Moore, R.E.; Paul, V.J. Lyngbyaloside B, a New Glycoside Macrolide from a Palauan Marine Cyanobacterium, *Lyngbya* sp. *J. Nat. Prod.* **2002**, *65*, 1945–1948. [[CrossRef](#)]
41. Klein, D.; Braekman, J.C.; Daloze, D.; Hoffmann, L.; Castillo, G.; Demoulin, V. Lyngbyapeptin A, a modified tetrapeptide from *Lyngbya bouillonii* (Cyanophyceae). *Tetrahedron Lett.* **1999**, *40*, 695–696. [[CrossRef](#)]
42. Luesch, H.; Yoshida, W.Y.; Moore, R.E.; Paul, V.J. Lyngbyastatin 2 and Norlyngbyastatin 2, Analogues of Dolastatin G and Nordolastatin G from the Marine Cyanobacterium *Lyngbya majuscula*. *J. Nat. Prod.* **1999**, *62*, 1702–1706. [[CrossRef](#)] [[PubMed](#)]

43. Mevers, E.; Matainaho, T.; Allara, M.; Di Marzo, V.; Gerwick, W.H. Mooreamide A: A cannabinomimetic lipid from the marine cyanobacterium *Moorea bouillonii*. *Lipids* **2014**, *49*, 1127–1132. [[CrossRef](#)] [[PubMed](#)]
44. Luesch, H.; Williams, P.G.; Yoshida, W.Y.; Moore, R.E.; Paul, V.J. Ulongamides A–F, New  $\beta$ -Amino Acid-Containing Cyclodepsipeptides from Palauan Collections of the Marine Cyanobacterium *Lyngbya* sp. *J. Nat. Prod.* **2002**, *65*, 996–1000. [[CrossRef](#)] [[PubMed](#)]
45. Levin, D.A. Alkaloid-bearing plants: An ecogeographic perspective. *Am. Nat.* **1976**, *110*, 261–284. [[CrossRef](#)]
46. Coley, P.D.; Aide, T.M. Comparison of herbivory and plant defenses in temperate and tropical broad-leaved forests. In *Plant–Animal Interaction: Evolutionary Ecology in Tropical and Temperate Regions*; Wiley-Interscience: New York, NY, USA, 1991; pp. 25–49.
47. Coley, P.D.; Barone, J.A. Herbivory and plant defenses in tropical forests. *Annu. Rev. Ecol. Syst.* **1996**, *27*, 305–335. [[CrossRef](#)]
48. Rasmann, S.; Agrawal, A.A. Latitudinal patterns in plant defense: Evolution of cardenolides, their toxicity and induction following herbivory. *Ecol. Lett.* **2011**, *14*, 476–483. [[CrossRef](#)]
49. Bakus, G.J.; Green, G. Toxicity in sponges and holothurians: A geographic pattern. *Science* **1974**, *185*, 951–953. [[CrossRef](#)]
50. Hay, M.E.; Fenical, W. Marine plant-herbivore interactions: The ecology of chemical defense. *Annu. Rev. Ecol. Syst.* **1988**, *19*, 111–145. [[CrossRef](#)]
51. Bolser, R.C.; Hay, M.E. Are tropical plants better defended? Palatability and defenses of temperate vs tropical seaweeds. *Ecology* **1996**, *77*, 2269–2286. [[CrossRef](#)]
52. Anstett, D.N.; Nunes, K.A.; Baskett, C.; Kotanen, P.M. Sources of Controversy Surrounding Latitudinal Patterns in Herbivory and Defense. *Trends Ecol. Evol.* **2016**, *31*, 789–802. [[CrossRef](#)] [[PubMed](#)]
53. Kooyers, N.J.; Blackman, B.K.; Holeski, L.M. Optimal defense theory explains deviations from latitudinal herbivory defense hypothesis. *Ecology* **2017**, *98*, 1036–1048. [[CrossRef](#)]
54. Shang, Z.; Winter, J.M.; Kauffman, C.A.; Yang, I.; Fenical, W. Salinipeptins: Integrated Genomic and Chemical Approaches Reveal D-Amino Acid-Containing Ribosomally Synthesized and Post-Translationally Modified Peptides from a Great Salt Lake *Streptomyces* sp. *ACS Chem. Biol.* **2019**, *14*, 415–425. [[CrossRef](#)] [[PubMed](#)]
55. Marcofelas, E.; Leung, T.; Okshevsky, M.; McKay, G.; Hignett, E.; Hamel, J.; Aguirre1, G.; Blenner-Hassett, O.; Boyle, B.; Lévesque, R.C.; et al. Culture-Dependent Bioprospecting of Bacterial Isolates From the Canadian High Arctic Displaying Antibacterial Activity. *Front. Microbiol.* **2019**, *10*, 1836. [[CrossRef](#)] [[PubMed](#)]
56. Bory, A.; Shilling, A.J.; Allen, J.; Azhari, A.; Roth, A.; Shaw, L.N.; Kyle, D.E.; Adams, J.H.; Amsler, C.D.; McClintock, J.B.; et al. Bioactivity of Spongian Diterpenoid Scaffolds from the Antarctic Sponge *Dendrilla antarctica*. *Mar. Drugs* **2020**, *18*, 327. [[CrossRef](#)]
57. Zhou, H.; He, Y.; Tian, Y.; Cong, B.; Yang, H. Bacilohydrin A, a New Cytotoxic Cyclic Lipopeptide of Surfactins Class Produced by *Bacillus* sp. SY27F from the Indian Ocean Hydrothermal Vent. *Nat. Prod. Commun.* **2019**, *14*, 141–146. [[CrossRef](#)]
58. Zhang, S.; Gui, C.; Shao, M.; Kumar, P.S.; Huang, H.; Ju, J. Antimicrobial tunicamycin derivatives from the deep sea-derived *Streptomyces xinghaiensis* SCSIO S15077. *Nat. Prod. Res.* **2020**, *34*, 1499–1504. [[CrossRef](#)]
59. Luzzatto-Knaan, T.; Garg, N.; Wang, M.; Glukhov, E.; Peng, Y.; Ackermann, G.; Amir, A.; Duggan, B.M.; Ryazanov, S.; Gerwick, L.; et al. Digitizing mass spectrometry data to explore the chemical diversity and distribution of marine cyanobacteria and algae. *eLife* **2017**, *6*, e24214. [[CrossRef](#)]
60. Naman, C.B.; Rattan, R.; Nikoulina, S.E.; Lee, J.; Miller, B.W.; Moss, N.A.; Armstrong, L.; Boudreau, P.D.; Debonsi, H.M.; Valeriote, F.A.; et al. Integrating molecular networking and biological assays to target the isolation of a cytotoxic cyclic octapeptide, samoamide A, from an American Samoan marine cyanobacterium. *J. Nat. Prod.* **2017**, *80*, 625–633. [[CrossRef](#)]
61. Crnkovic, C.M.; May, D.S.; Orjala, J. The impact of culture conditions on growth and metabolomic profiles of freshwater cyanobacteria. *J. Appl. Phycol.* **2018**, *30*, 375–384. [[CrossRef](#)]
62. Pallarés, N.; Tolosa, J.; Mañes, J.; Ferrer, E. Occurrence of Mycotoxins in Botanical Dietary Supplement Infusion Beverages. *J. Nat. Prod.* **2019**, *82*, 403–406. [[CrossRef](#)] [[PubMed](#)]
63. Engene, N.; Tronholm, A.; Paul, V.J. Uncovering cryptic diversity of *Lyngbya*: The new tropical marine cyanobacterial genus *Dapis* (Oscillatoriales). *J. Phycol.* **2018**, *54*, 435–446. [[CrossRef](#)]
64. Jayaram, B.; Klawonn, F. Can unbounded distance measures mitigate the curse of dimensionality? *Int. J. Data Min. Model. Manag.* **2012**, *4*, 361–383. [[CrossRef](#)]

65. Milligan, K.E.; Márquez, B.; Williamson, R.T.; Davies-Coleman, M.; Gerwick, W.H. Two New Malyngamides from a Madagascan *Lyngbya majuscula*. *J. Nat. Prod.* **2000**, *63*, 965–968. [[CrossRef](#)] [[PubMed](#)]
66. Edwards, D.J.; Marquez, B.L.; Nogle, L.M.; McPhail, K.; Goeger, D.E.; Roberts, M.A.; Gerwick, W.H. Structure and Biosynthesis of the Jamaicamides, New Mixed Polyketide-Peptide Neurotoxins from the Marine Cyanobacterium *Lyngbya majuscula*. *Chem. Biol.* **2004**, *11*, 817–833. [[CrossRef](#)] [[PubMed](#)]
67. Linington, R.G.; Clark, B.R.; Trimble, E.E.; Almanza, A.; Ureña, L.D.; Kyle, D.E.; Gerwick, W.H. Antimalarial Peptides from Marine Cyanobacteria: Isolation and Structural Elucidation of Gallinamide A. *J. Nat. Prod.* **2009**, *72*, 14–17. [[CrossRef](#)] [[PubMed](#)]
68. Negishi, E.; Tan, Z.; Liang, B.; Novak, T. An efficient and general route to reduced polypropionates via Zr-catalyzed asymmetric C-C bond formation. *Proc. Natl. Acad. Sci. USA* **2004**, *101*, 5782–5787. [[CrossRef](#)]
69. Pereira, A.; Etzbach, L.; Engene, N.; Müller, R.; Gerwick, W.H. Molluscicidal Metabolites from an Assemblage of Palmyra Atoll Cyanobacteria. *J. Nat. Prod.* **2011**, *74*, 1175–1181. [[CrossRef](#)]
70. Boudreau, P.D.; Byrum, T.; Liu, W.T.; Dorrestein, P.C.; Gerwick, W.H. Viequeamide A, a Cytotoxic Member of the Kulolide Superfamily of Cyclic Depsipeptides from a Marine Button Cyanobacterium. *J. Nat. Prod.* **2012**, *75*, 1560–1570. [[CrossRef](#)]
71. Hooper, G.J.; Orjala, J.; Schatzman, R.C.; Gerwick, W.H. Carmabins A and B, New Lipopeptides from the Caribbean Cyanobacterium *Lyngbya majuscula*. *J. Nat. Prod.* **1998**, *61*, 529–533. [[CrossRef](#)]
72. Moss, N.A.; Seiler, G.; Leão, T.F.; Castro-Falcón, G.; Gerwick, L.; Hughes, C.C.; Gerwick, W.H. Nature's Combinatorial Biosynthesis Produces Vatiamides A–F. *Angew. Chem. Int. Ed.* **2019**, *58*, 9027–9031. [[CrossRef](#)] [[PubMed](#)]
73. Gerwick, W.H.; Tan, L.T.; Sitachitta, N. Nitrogen-containing metabolites from marine cyanobacteria. In *The Alkaloids: Chemistry and Biology*, 1st ed.; Cordell, G.A., Ed.; Academic Press: Cambridge, MA, USA, 2001; Volume 57, pp. 75–184. [[CrossRef](#)]
74. Tidgewell, K.; Clark, B.R.; Gerwick, W.H. The Natural Products Chemistry of Cyanobacteria. In *Comprehensive Natural Products II: Chemistry and Biology*, 1st ed.; Mander, L.N., Liu, H.-W., Eds.; Elsevier: Amsterdam, The Netherlands, 2010; Volume 2, pp. 144–188. [[CrossRef](#)]
75. Zhang, C.; Idelbayev, Y.; Roberts, N.; Tao, Y.; Nannapaneni, Y.; Duggan, B.M.; Min, J.; Lin, E.C.; Gerwick, E.C.; Cottrell, G.W.; et al. Small Molecule Accurate Recognition Technology (SMART) to Enhance Natural Products Research. *Sci. Rep.* **2017**, *7*, 14243. [[CrossRef](#)]
76. Sadar, M.D.; Williams, D.E.; Mawji, N.R.; Patrick, B.O.; Wikanta, T.; Chasanah, E.; Irianto, H.E.; Van Soest, R.; Andersen, R.J. Sintokamides A to E, Chlorinated Peptides from the Sponge *Dysidea* sp. that Inhibit Transactivation of the N-Terminus of the Androgen Receptor in Prostate Cancer Cells. *Org. Lett.* **2008**, *10*, 4947–4950. [[CrossRef](#)]
77. Lowery, C.A.; Park, J.; Gloeckner, C.; Meijler, M.M.; Mueller, R.S.; Boshoff, H.I.; Ulrich, R.L.; Barry, C.E.; Bartlett, D.H.; Kravchenko, V.V.; et al. Defining the Mode of Action of Tetramic Acid Antibacterials Derived from *Pseudomonas aeruginosa* Quorum Sensing Signals. *J. Am. Chem. Soc.* **2009**, *131*, 14473–14479. [[CrossRef](#)]
78. Ricciotti, E.; FitzGerald, G.A. Prostaglandins and Inflammation. *Arterioscler. Thromb. Vasc. Biol.* **2011**, *31*, 986–1000. [[CrossRef](#)] [[PubMed](#)]
79. Stokes, J.M.; Yang, K.; Swanson, K.; Jin, W.; Cubillos-Ruiz, A.; Donghia, N.M.; MacNair, C.R.; French, S.; Carfrae, L.A.; Bloom-Ackermann, Z.; et al. A Deep Learning Approach to Antibiotic Discovery. *Cell* **2020**, *181*, 475–483. [[CrossRef](#)]
80. Moss, N.A.; Leao, T.; Glukhov, E.; Gerwick, L.; Gerwick, W.H. Collection, Culturing, and Genome Analyses of Tropical Marine Filamentous Benthic Cyanobacteria. In *Methods in Enzymology*, 1st ed.; Tawfik, D.S., Ed.; Academic Press: Cambridge, MA, USA, 2018; Volume 604, pp. 3–43. [[CrossRef](#)]
81. Van Rossum, G.; Drake, F.L., Jr. *Python Reference Manual, Release 2.0.1*; PythonLabs: Amsterdam, The Netherlands, 1995; Available online: <https://docs.python.org/2.0/ref/ref.html> (accessed on 14 October 2020).
82. McKinney, W. Data Structures for Statistical Computing in Python. In Proceedings of the 9th Python in Science Conference (SciPy2010), Austin, TX, USA, 28 June–3 July 2010; pp. 51–56. [[CrossRef](#)]
83. Pandas-Dev/Pandas, Version v0.25.2, 2018, Zenodo. Available online: <https://doi.org/10.5281/zenodo.3509135> (accessed on 14 October 2020).
84. Oliphant, T.E. *A Guide to NumPy*, 2nd ed.; Trelgol Publishing: USA, 2006; Available online: <https://web.mit.edu/dvp/Public/numpybook.pdf> (accessed on 14 October 2020).



85. van der Walt, S.; Colbert, S.C.; Varoquaux, G. The NumPy Array: A Structure for Efficient Numerical Computation. *Comput. Sci. Eng.* **2011**, *13*, 22–30. [[CrossRef](#)]
86. Goloborodko, A.A.; Levitsky, L.I.; Ivanov, M.V.; Gorshkov, M.V. Pyteomics—A Python Framework for Exploratory Data Analysis and Rapid Software Prototyping in Proteomics. *J. Am. Soc. Mass Spectr.* **2013**, *24*, 301–304. [[CrossRef](#)] [[PubMed](#)]
87. Levitsky, L.I.; Klein, J.; Ivanov, M.V.; Gorshkov, M.V. Pyteomics 4.0: Five years of development of a Python proteomics framework. *J. Proteome Res.* **2019**, *18*, 709–714. [[CrossRef](#)] [[PubMed](#)]
88. Virtanen, P.; Gommers, R.; Oliphant, T.E.; Haberland, M.; Reddy, T.; Cournapeau, D.; Burovski, E.; Peterson, P.; Weckesser, W.; Bright, J.; et al. SciPy 1.0: Fundamental algorithms for scientific computing in Python. *Nat. Methods* **2020**, *17*, 261–272. [[CrossRef](#)]
89. Hagberg, A.A.; Schult, D.A.; Swart, P.J. Exploring network structure, dynamics, and function using NetworkX. In Proceedings of the 7th Python in Science Conference (SciPy2008), Pasadena, CA, USA, 19–24 August 2008; pp. 11–15.
90. Hunter, J.D. Matplotlib: A 2D graphics environment. *Comput. Sci. Eng.* **2007**, *9*, 90–95. [[CrossRef](#)]
91. Pedregosa, F.; Varoquaux, G.; Gramfort, A.; Michel, V.; Thirion, B.; Grisel, O.; Blondel, M.; Prettenhofer, P.; Weiss, R.; Dubourg, V.; et al. Scikit-learn: Machine Learning in Python. *J. Mach. Learn. Res.* **2011**, *12*, 2825–2830.
92. Mwachom/Seaborn, v0.9.0. 2018. Available online: <https://doi.org/10.5281/zenodo.1313201> (accessed on 14 October 2020).
93. Pérez, F.; Granger, B.E. IPython: A System for Interactive Scientific Computing. *Comput. Sci. Eng.* **2007**, *9*, 21–29. [[CrossRef](#)]
94. Kluyver, T.; Ragan-Kelley, B.; Pérez, F.; Granger, B.; Bussonnier, M.; Frederic, J.; Kelley, K.; Hamrick, J.; Grout, J.; Corlay, S.; et al. Jupyter Notebooks—A publishing format for reproducible computational workflows. In *Positioning and Power in Academic Publishing: Players, Agents and Agendas*; Loizides, F., Schmidt, B., Eds.; IOS Press: Amsterdam, The Netherlands, 2016; pp. 87–90. [[CrossRef](#)]
95. Holman, J.D.; Tabb, D.L.; Mallick, P. Employing ProteoWizard to Convert Raw Mass Spectrometry Data. *Curr. Protoc. Bioinform.* **2014**, *46*, 1–9. [[CrossRef](#)]
96. Chambers, M.C.; Maclean, B.; Burke, R.; Amodei, D.; Ruderman, D.L.; Neumann, S.; Gatto, L.; Fischer, B.; Pratt, B.; Egertson, J. A cross-platform toolkit for mass spectrometry and proteomics. *Nat. Biotechnol.* **2012**, *30*, 918–920. [[CrossRef](#)]
97. Shannon, P.; Markiel, A.; Ozier, O.; Baliga, N.S.; Wang, J.T.; Ramage, D.; Amin, N.; Schwikowski, B.; Ideker, T. Cytoscape: A software environment for integrated models of biomolecular interaction networks. *Genome Res.* **2003**, *13*, 2498–2504. [[CrossRef](#)]
98. Iwasaki, A.; Ohno, O.; Sumimoto, S.; Ogawa, H.; Nguyen, K.A.; Suenaga, K. Jahanyne, an Apoptosis-Inducing Lipopeptide from the Marine Cyanobacterium *Lyngbya* sp. *Org. Lett.* **2015**, *17*, 652–655. [[CrossRef](#)]
99. Linington, R.G.; González, J.; Ureña, L.D.; Romero, L.I.; Ortega-Barría, E.; Gerwick, W.H. Venturamides A and B: Antimalarial Constituents of the Panamanian Marine Cyanobacterium *Oscillatoria* sp. *J. Nat. Prod.* **2007**, *70*, 397–401. [[CrossRef](#)]
100. Yoshimura, A.; Kishimoto, S.; Nishimura, S.; Otsuka, S.; Sakai, Y.; Hattori, A.; Takeya, H. Prediction and Determination of the Stereochemistry of the 1,3,5-Trimethyl-Substituted Alkyl Chain in Verucopeptin, a Microbial Metabolite. *J. Org. Chem.* **2014**, *79*, 6858–6867. [[CrossRef](#)]
101. Tao, Y.; Li, P.; Zhang, D.; Glukhov, E.; Gerwick, L.; Zhang, C.; Murray, T.F.; Gerwick, W.H. Samholides, Swinholide-Related Metabolites from a Marine Cyanobacterium cf. *Phormidium* sp. *J. Org. Chem.* **2018**, *83*, 3034–3046. [[CrossRef](#)]

102. Choi, H.; Mascuch, S.J.; Villa, F.A.; Byrum, T.; Teasdale, M.E.; Smith, J.E.; Preskitt, L.B.; Rowley, D.C.; Gerwick, L.; Gerwick, W.H. Honaucins A-C, potent inhibitors of inflammation and bacterial quorum sensing: Synthetic derivatives and structure-activity relationships. *Chem. Biol.* **2012**, *19*, 589–598. [[CrossRef](#)] [[PubMed](#)]
103. Green, L.C.; Wagner, D.A.; Glogowski, J.; Skipper, P.L.; Wishnok, J.S.; Tannenbaum, S.R. Analysis of nitrate, nitrite, and [N-15]-labeled nitrate in biological-fluids. *Anal. Biochem.* **1982**, *126*, 131–138. [[CrossRef](#)]

**Publisher’s Note:** MDPI stays neutral with regard to jurisdictional claims in published maps and institutional affiliations.



© 2020 by the authors. Licensee MDPI, Basel, Switzerland. This article is an open access article distributed under the terms and conditions of the Creative Commons Attribution (CC BY) license (<http://creativecommons.org/licenses/by/4.0/>).